UNIVERSITY OF COPENHAGEN
FACULTY OF SCIENCE

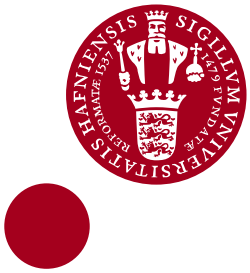

Master's Thesis

Fluctuation-induced motility of topological defects

Lasse Bonn

Advisor: Amin Doostmohammadi

Date: 20th May 2022

Acknowledgement

First and foremost, I want to thank Amin, for introducing me to the world of active matter, giving me the opportunity to be part of such a great project and guiding me throughout. Thank you also to Sasha, for help and helpful words and Benjamin for help with some long equations. Many thanks to Romain for the excellent codebase. Finally, many thanks to Sorcha, my friends, family and office mates for the energy to keep going.

Abstract

Topological defects are increasingly being identified in a wide range of biological systems and are being revealed to play a functional role in diverse biological processes such as cell death, tissue regeneration and bacterial invasion. The emergence of such topological defects has led to interesting analogies with nematic liquid crystals and are widely associated with the activity, i.e. the ability of living systems to continuously exert mechanical forces on their environment. In this work, we show that even for a passive nematic, fluctuations in orientation or velocity, along with elastic effects, can result in defects showing self propulsion and stress patterns similar to those observed in experiments on biological systems and in models of active nematics. Using continuum simulations of fluctuating nematohydrodynamics, we can reproduce the self-propelled defect chaos phase, characteristic of active nematics. Both hydrodynamic and orientational fluctuations reproduce this phase along with the flow patterns and the isotropic stress patterns. We show the possibility of both extensile and contractile defect motion arising from fluctuations and the essential role that elastic effects play in establishing this new phenomenon. These findings question the current consensus that activity is the main driver of motile topological defects in biological systems and open the door to new sets of theoretical and experimental studies to distinguish between fluctuation-induced and active behaviour in living materials.

Contents

1 Introduction

There is now growing evidence of the emergence of liquid crystalline features in biological systems (see [1] for a recent review). Significant among others is the nematic orientational order, manifest in the form of collective alignment along particular axes [2], which is observed in subcellular filaments [3–6], bacterial biofilms [7–9], and cell monolayers [10, 11]. Due to the head-tail symmetry of the nematic particles, the lowest energy defects are of topological charge $\pm 1/2$, meaning that as one traces a loop around the defect, the particles rotate by $\pm\pi$. Topological defects in nematics have recently been found to be at the core of many biological functions, e.g. cell extrusion in mammalian epithelia [10], neural mound formation [12] and limb origination in the simple animal *Hydra* [6] (see [1, 13, 14] for recent reviews on physical and biological significance of topological defects).

What sets these biological nematics apart from their passive counterparts is the presence of activity: each constituent element of living matter is capable of producing work and injecting energy locally by means of active stress generation [15]. While the existence of quasi long-range order has also been proven for active nematics [16, 17], the dynamical properties of defects are expected to be different from the passive case since, as a consequence of activity, the $+1/2$ defects with polar symmetry can self-propel and move along their axis of symmetry [18]. These comet-shaped $+1/2$ defects are characterised by a head region where the director field predominantly bends and a tail region where splay is dominant. For an extensile active stress, which extends along the elongation direction of active particles, the resulting motion of $+1/2$ defects is along the head, while the opposite holds for contractile active stresses that tend to point inwards along the elongation axis of active particles [18]. This persistent movement, both in the direction of the head and the tail of the $+1/2$ defect, has been observed in various biological systems, e.g. contractile in fibroblasts [11] and extensile in epithelial monolayers [10]. Recently it has even been shown that perturbing the adhesion between cells can result in a switch between extensile and contractile behaviours in epithelial cell layers [19]. While the emergence of extensile or contractile behaviour of topological defects has been widely associated to the activity of these systems, here we show that fluctuations can lead to similar patterns of flows around topological defects and result in both extensile and contractile defect behaviour.

In passive nematics, fluctuations are known to drive the Berezinskii–Kosterlitz–Thouless (BKT) transition, in which spontaneously generated topological defects unbind to break the quasi long-range order [20]. This has been analytically shown for a 2-dimensional passive, dry nematic, by renormalisation group analyses [21]. Computational studies have shown the BKT transition for 2D passive nematics with a lattice model with finite size scaling [22], and for a dry, freely moving, particle-based model for various length to width ratios [23, 24]. A similar BKT type transition was also reported in a discrete model of active nematics [25].

Drawing analogies with the BKT transition in passive nematics, it has been shown that in over-damped active nematics, where hydrodynamic flows are dominated and suppressed by frictional screening, self-propulsion of $\pm 1/2$ topological defects can lead to the defect pair unbinding, destroying any (quasi) long-range orientational order [26]. Introducing fluctuating forces coupled to the nematic alignment field, it was lately shown that such specific fluctuations can result in an effective extensile stresses in passive nematics [27]. More recently, combining discrete, vertex-based, simulations of model cellular layers with analytical treatment of linearised nematohydrodynamics equations, it has even been argued that any fluctuations can result in the appearance of "active" extensile or contractile nematics, depending on the flow-aligning behaviour of the particles [28]. Similarly, cell shape fluctuations in a cell-based, phase-field, model of cell monolayer has been shown to affect self-propulsive features of topological defects [29]. Notwithstanding these recent works, the dynamics and flow features of topological defects in the presence of fluctuations remain poorly understood. Moreover, it is not clear how different sources of fluctuations in hydrodynamic flows and in particle alignment affect the creation, annihilation, and motion of topological defects in the absence of any active stresses and whether fluctuations alone can explain experimental observations of contractile- and extensile-like defect motions in cellular layers. Here, we aim to fill this gap and address this challenge using continuum model of active nematics in the presence of various sources of fluctuations.

We will now introduce some key concepts of the current work which will be recurring themes throughout the thesis.

Active matter is a unique class of matter in that the particles themselves perform work.

This sets it apart, qualitatively, from passive matter and allows for a wide range of interesting collective phenomena [15]. Examples of active matter are as diverse as actin myosin mixtures [30], epithelia [6, 10], or fish swarms and bird flocks [31]. As the examples illustrate, active matter is a popular model for describing collective behaviour in living systems, showing such behaviours as flocking [15], giant number fluctuations [32], motility induced phase transitions [33] and much more.

Active nematics is a sub field of active matter, dealing with apolar particles. Nematics are liquid crystals in which there is no positional order (liquid), but orientational order (crystal) [20]. Active nematics extends nematics by adding an active stress which acts in the directions of the orientation [18]. This active stress leads to a phase called active turbulence, in which self-propelled topological defects are constantly generated and annihilate again, stirring up the fluid [18, 34]. Experimental active nematics systems have been developed, for example actin-myosin or kinesin-microtubule mixtures [30] which have made it possible to observe the active turbulence phase [4], defect behaviours [35] and emergent length scales and scaling

laws [36]. Experimental active nematics is backed by a large body of theoretical work from micro scale particle descriptions [37] to large scale continuum simulations [2, 38]. But active nematics are not purely a toy model system, as many real world systems have shown to behave as active nematics [1, 39, 40] including mouse fibroblasts [11, 41] or bacterial colonies [42].

Topological defects are topologically protected regions of the nematic, where the order vanishes [20]. Due to their long lifetime and effect on the nematic field, they play a large role in the behaviour of nematics. One key feature of active nematics is its inherent instability to splay or bend depending on the sign of the active stress, found by Aditi Simha and Ramaswamy [43] which leads to active turbulence and unbinding of topological defect pairs, in an active analogue of the defect unbinding (BKT) transition [14]. What sets defects in active nematics apart, is that they are self propelled and so affect their surroundings dynamically [18]. These topological defects have been widely studied and shown to be of real biological significance [1, 13], e.g. in MDCK epithelia [10], neural progenitor cells [12] and biofilms of elongated bacteria [9].

Motile defects have been widely observed in mammalian cells. Weakly active mouse fibroblasts have shown motile defects [11, 41] as well as human bronchial epithelia [44]. In fact, in Madin-Darby canine kidney cells (MDCK), topological defects were found to effect the extrusion of cells from the epithelial monolayer [10]. The epithelium exists in a state called dynamic homeostasis, a steady state in which new cells enter the epithelium and other cells, e.g. damaged or aged, are extruded from the cell layer. This dynamics must be preserved to keep the epithelium healthy. Saw et al. [10] found motile topological defects in the layer and showed that the stress patterns (Figures 1 and 8) exhibited by $+1/2$ defects were the cause of cell extrusion.

A study on neural progenitor cells, which are stem cells that can develop into the central nervous system, showed that these cells organise nematically with topological defects visible [12]. These defects were motile with the expected flow patterns and created a defect chaos phase. Additionally, cells accumulated at $+1/2$ defects and formed mounds, possibly functional features, as well as decreased cell density at $-1/2$ defects (Figure 1).

In a similar observation, Copenhagen et al. [9] found that $+1/2$ and $-1/2$ defects play opposite roles in extra layer formation in a single layer biofilm of rod shaped *Myxococcus* bacteria. Specifically, they found that $+1/2$ defects lead to a new layer forming on top of the layer the defect is in, whereas $-1/2$ defects create a hole in the layer, leading to one less layer at that point. They explained this behaviour by imposing anisotropic friction (a cell moving along its axis would feel less friction that one moving perpendicular to its long axis) and finding that $+(-)1/2$ defects have net in (out) flow, meaning that the cells must escape to a new layer (flee the defect). A recent study on MDCK layers has confirmed the hole formation effect of $-1/2$ defects

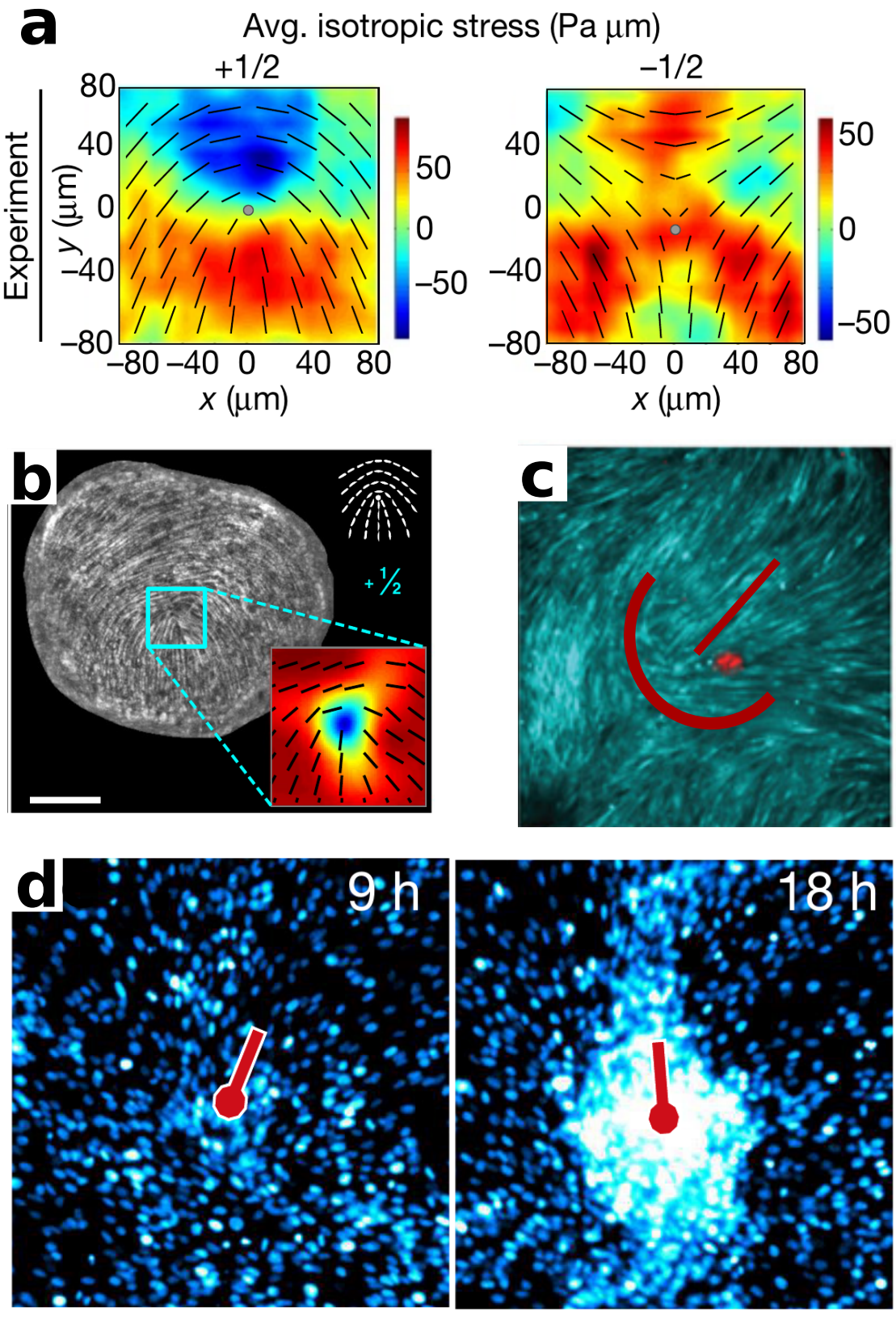

(Caption on next page.)

Figure 1: Functional topological defects in biological systems.
a shows isotropic stress fields of $\pm 1/2$ defects in mammalian epithelial monolayers where $+1/2$ defects were found to lead to cell extrusion. From [10]. **b** shows a $+1/2$ defect playing a role in *Hydra* morphogenesis. From [6]. **c** shows a tumour spheroid (red) as it tries to invade the mesothelium (blue) and is impeded by the $+1/2$ defect. From [45]. **d** In neural progenitor cells, $+1/2$ defects lead to mound formation. From [12].

for mammalian epithelia [46].

A study on ovarian cancer cells found that topological defect flow affected the cancer invasion called mesothelial clearance [45]. During mesothelial clearance, a tumour must clear the cells in the mesothelium to make space for itself. The authors found that for three types of ovarian cancer, if the tumour tries to invade near a $+1/2$ topological defect, the clearance will be > 2 times slower than in a control area (Figure 1).

Topological defects have also been shown to play a central role in morphogenesis. In *Hydra*, defects determine the location of the mouth and and head of the developing animal [6] (Figure 1).

An experiment on MDCK cells switched the behaviour of the tissue from extensile to contractile by knocking out E-cadherin, a protein that binds cells together [19]. This means that the defect flow field was reversed. Surprisingly, the defect isotropic stress pattern did not reverse. This means that the isotropic stress pattern is not solely determined by flow.

Fluctuations are always present in biology [47], as thermal noise or other sources of randomness, and have been found to affect and effect many processes. At the cellular level, fluctuations in genetic circuits plays a crucial role in stochastic processes such as differentiation or state switching [48] and organoid development [49], at the tissue or population level these stochastic behaviours can mean a wider geno- or phenotype pool leading to more resilient populations [48]. It may be noted that an extended gene pool is the prerequisite for evolution. On a larger scale, fluctuations in ecology can lead to long term oscillations [50] or transitions between states in lakes [51]. So fluctuations may refer to stochastic inputs to the system as well as stochastic behaviours.

Fluctuations on the cellular level in cellular systems have been widely documented, with many theoretical studies on e.g. fluidisation [52], but experimental quantification of fluctuations has not followed suit. There are a few types of fluctuations that could be considered relevant. Epithelial cells are constantly probing their environment [53, 54] which entails developing focal adhesions to the substrate and applying forces which were found to vary > 1.5 fold several times per minute [55]. In confluent cell layers,

the so called $T1$ transition swaps neighbours and in doing so affects the cell shape. This $T1$ transition has been shown to be dependent on fluctuating junction lengths, themselves affecting cell shape [56]. More generally, cell areas have been shown to vary strongly, up to 20%, amounting to large shape changes [57]. Possibly most relevant to this study, alignment of cells during periodic perpendicular stretching was modelled with an alignment term plus a random noise in the orientation [58]. This revealed an orientational noise where the authors determined a diffusion constant. Although these cells are alone, not confluent, the diffusion constant may well be useful and is discussed in the fluctuation strength discussion section.

With a few exceptions [25, 59], the effect of fluctuations on active nematics has not been much studied, presumably due to difficulties in analytical and computational treatment. Recently, Killeen, Bertrand and Lee [28] found analytically and verified the generation of self propelled defects in a passive nematic by fluctuations using a vertex model.

In this work, we present computational results showing that fluctuations in nematic orientation or fluid velocity can lead to self propelled defects in a passive nematic.

We will first cover the theory behind the phenomenological approach to nematics. We then review the relevant literature, discussing results in active nematics and noisy nematics. Next, we discuss computational methods and the model parameters and fluctuation implementations are introduced.

We then present results which show self propelled topological defects in a noisy, passive nematic with hydrodynamical interactions, where we recover experimentally observed stress and velocity fields. The effect of fluctuation strength and flow alignment are investigated. We also show the influence of different values for bend and splay elastic constants.

Finally, a short conclusion summarises and contextualises the work done and outlines possible future directions. It is worth noting, that the section on the generation of motile defects by fluctuations has been developed as a paper, available at [60], which is currently under revision at *PRL*.

2 Theoretical background

In this section we first develop the theory behind nematics modelling, then extend to wet, active nematics. We then go into the details of topological defects.

2.1 Nematics

Nematics are a class of liquid crystal in which there is no positional order, but order in the orientation [20]. It is important to note that a nematic particle is apolar but has two-fold symmetry. An example would be an oval, whereas counterexamples would be an arrow (polar) or a sphere (no orientation) or a triangle (3-atic).

We restrict ourselves to 2 dimensional nematics, which has several implications which will become clear over the course of the following description. In 2 dimensions, the orientation of the nematic can simply be described by a scalar $\theta \in [0, \pi)$, which represents the angle of the nematic. We therefore are dealing with uniaxial nematics, and do not need to consider biaxial nematics. This results in an order parameter space of half a unit circle, with the points $\theta = 0$ and $\theta = \pi$ identified.

We describe the orientation of the nematic with a headless unit length vector called the director $\vec{n} = -\vec{n}$, which takes into account the apolarity of the nematic (Figure 2).

Defining the angle between the director $\vec{n}$ and the orientation of the i-th particle θ_i as α, we can define the order as [61]:

$$S = \frac{1}{2} < 3\cos(\alpha_i)^2 - 1 > \tag{1}$$

where $< ... >$ denotes averaging over all particle orientations.

Averaging for the whole system would give the order in polar systems, however, in nematics, when taking nonzero temperatures into account, averaging over an infinite system leads to $S \to 0$. This is because according to the Mermin-Wagner-Berezenskii theorem, there cannot be long range order in a system with continuous symmetry [20]. In a nematic, the order decays algebraically, which is known as quasi long-range order and has been shown also for passive [23] and active nematics [25]. Therefore averaging must be local even at low temperatures.

While it can sometimes be easier to use the director [34, 43], a separate equation must be formulated for the order S. An order parameter which contains all the information about orientation and order of the nematic can be constructed as:

$$Q_{ij} = \frac{S}{2}(n_i n_j - \frac{\delta_{ij}}{2}), \tag{2}$$

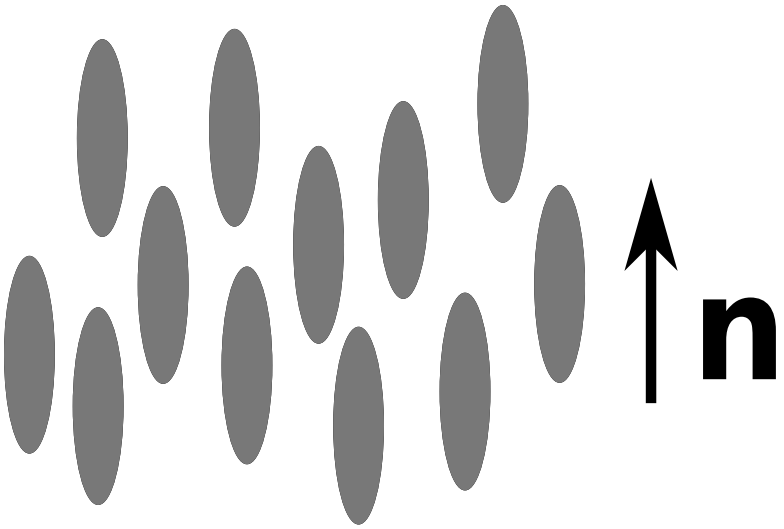

Figure 2: Nematic phase with director $\vec{n}$. The particles have no positional order but all have the same orientation.

therefore we will only need one equation to follow the evolution of the nematic. In this way, $\mathbf{Q}$ is a symmetric traceless tensor which captures the orientation of the nematic (eigenvector corresponding to the largest eigenvalue) and the strength of the order (S). We note that in 2D the order can be computed by $S = \sqrt{Q_{xx}^2 + Q_{yy}^2}$.

2.1.1 Landau free energy

We can now construct a Landau free energy, using the *Landau-de Gennes expansion* [62]. Because the free energy is invariant under rotations of the director or the coordinate system and $\mathbf{Q}$ is not, we expand in powers of $\operatorname{Tr}\mathbf{Q}$ [20, 63]:

$$\begin{aligned} f_{\mathrm{L}} &= C_1 \operatorname{Tr}\mathbf{Q} + C_2 \operatorname{Tr}\mathbf{Q}^2 + C_3 \operatorname{Tr}\mathbf{Q}^3 + C_4 \operatorname{Tr}\mathbf{Q}^4 \\ &= C_2 \operatorname{Tr}\mathbf{Q}^2 + C_4 \operatorname{Tr}\mathbf{Q}^4. \end{aligned} \tag{3}$$

Note that, by definition $\operatorname{Tr}\mathbf{Q} = 0$. It follows that, in 2D, $\operatorname{Tr}\mathbf{Q}^3 = 0$ which precludes the typical first order Landau theory isotropic-nematic transition. We combine C_2 and C_4 to make the coupling constant C and the Landau free energy reads:

$$f_L = C(1 - \operatorname{Tr}\mathbf{Q}^2)^2 \tag{4}$$

2.1.2 Elastic free energy

Elastic effects also play a role which are taken into account by the so-called Frank free energy [20]. The Frank elastic free energy is most simply formulated in terms of $\vec{n}$, and it is easier to understand the terms this way. A general linear stiffness K_{ijkl}, will take into account all relations between gradients of $\vec{n}$:

$$f_{el} = K_{ijkl}\partial_i n_j \partial_k n_l. \tag{5}$$

However, symmetry considerations allow us to reduce K_{ijkl} to 3 components [20], $k_{1,2,3}$:

$$f_{el} = k_1(\nabla \cdot \vec{n})^2 + k_2(\vec{n} \cdot (\nabla \times \vec{n}))^2 + k_3(n \times (\nabla \times n))^2 \tag{6}$$

So $k_{1,2,3}$ are coefficients for three types of deformation called splay, twist and bend respectively (Figure 3). Splay occurs when the neighbour perpendicular to the director rotates. Twist occurs when when one of two neighbouring parallel particles rotates out of plane into the third dimension, not possible in two dimensions. Bend occurs when the neighbour in the direction of the director rotates.

We therefore keep splay and bend terms with constants k_1 and k_3.

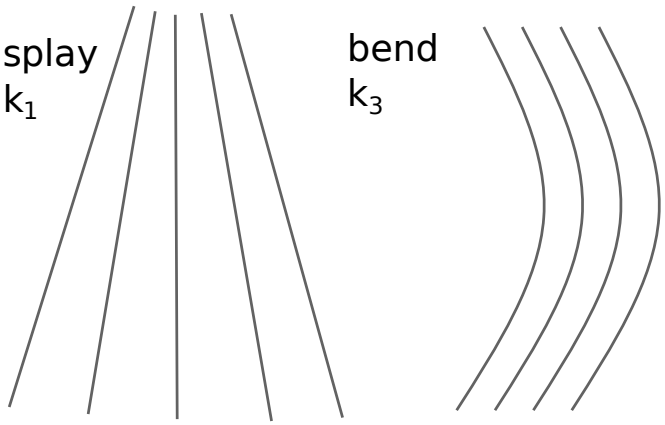

Figure 3: Illustration of splay and bend deformations. Here we have drawn tangent lines to the particles. When the field splays, neighbours in the director direction have the same orientation, whereas when the field bends, neighbours perpendicular to the director direction (along the long side) have the same orientation. k_1 and k_3 quantify the resistance of the nematic to splay and bend deformations, respectively.

However, we phrase our model in terms of $\mathbf{Q}$ and so we need to find an expression in $\mathbf{Q}$. When using the elastic energy in terms of $\mathbf{Q}$, an approximation with only one term using $K = k_1 = k_3$ is commonly employed [13, 18, 34]:

$$f_{el} = \frac{K}{2}\partial_k Q_{ij}\partial_k Q_{ij}, \tag{7}$$

capturing divergence in $\mathbf{Q}$. For simplicity, we use this approach when not investigating the effect of different elastic constants.

In this work we were also interested in exploring the effect of differing splay and bend coefficients, however, this description does not allow for varying response to splay vs respond to bend. Therefore we follow Edwards and Beris [64, 65] in using three terms, one for each bend, splay and twist:

$$f_{el} = \frac{L_1}{2}\partial_k Q_{ik}\partial_l Q_{il} + \frac{L_2}{2}\partial_k Q_{ij}\partial_k Q_{ij} + \frac{L_3}{2}Q_{ij}\partial_i Q_{kl}\partial_j Q_{kl}. \tag{8}$$

We now have a one-to-one correspondence between $k_{1,2,3}$ and $L_{1,2,3}$ as follows [65, 66]:

$$L_1 = \frac{-k_1 + 2k_2 + k_3}{4S^2} = \frac{-k_1 + k_3}{4S^2} \tag{9a}$$

$$L_2 = \frac{k_1 - k_2}{S^2} = \frac{k_1}{S^2} \tag{9b}$$

$$L_3 = \frac{-k_1 + k_3}{2S^3} = \frac{-k_1 + k_3}{2S^3} \tag{9c}$$

Now we can describe the model in terms of the more common and intuitive k constants while using the more computationally useful L constants. We set $k_2 = 0$ and obtain expressions for L_i. Although we only have two k constants, we keep the L_3 term and investigate its effect. Note that we recover the single constant approximation (7) when $k_1 = k_3$.

2.1.3 Molecular field

Having developed the expression for Landau type and elastic free energy, the total free energy is simply a sum thereof:

$$f_{nem} = f_L + f_{el} \tag{10}$$

$$= C(1 - \operatorname{Tr} \mathbf{Q}^2)^2 + \frac{K}{2}(\nabla \mathbf{Q})^2, \tag{11}$$

for the single elastic constant approximation. We can then define a molecular field $\mathbf{H}$, the negative, symmetric, traceless part of the functional derivative of $\mathbf{Q}$:

$$\mathbf{H} = -\left(\frac{\delta \mathcal{F}}{\delta \mathbf{Q}}\right)^{ST}, \tag{12}$$

where $\delta a / \delta b$ is the functional derivative. The molecular field therefore is an equilibrating force. We use the molecular field to determine the dynamics of the nematic. A dry nematic has only these interactions, whereas a wet nematic also interacts hydrodynamically with the solvent.

The time evolution of the nematic then follows:

$$\frac{D\mathbf{Q}}{Dt} = \Gamma \mathbf{H}, \tag{13}$$

where D/Dt is the co-moving, co-rotational derivative and Γ is the rotational diffusivity. So this is simply relaxational dynamics to the free energy minimum.

2.2 Wet nematics

We have introduced so called dry nematics, with only nematic interactions. A *wet nematic* is constructed by adding a hydrodynamical field and coupling it to the

nematic field. The fluid velocity evolution follows incompressible Navier-Stokes with a generic stress:

$$\rho(\partial_t \vec{v} + \vec{v} \cdot \nabla \vec{v}) = \nabla \cdot \mathbf{\Pi}, \quad \nabla \cdot \vec{v} = 0. \tag{14}$$

The generic stress, $\mathbf{\Pi}$, includes pressure and the typical viscose term (22) and an elastic term (23) which couples the flow to the nematic field.

The coupling between the nematic and the flow field is called backflow and is modulated by the *flow alignment* parameter, ξ. The backflow is present in both the nematic evolution (13) and the fluid evolution (14). Regulating the influence of flow on the nematic, ξ modulates the influence of the strain rate vs the vorticity on $\mathbf{Q}$ in (20). On the other hand, the influence of the nematic field on the fluid velocity is captured in the elastic stress term (23). The effect of the flow alignment parameter can be understood as follows: for a threshold value ξ_c, when $|\xi| < \xi_c$ the particle will tumble in the flow, whereas when $|\xi| > \xi_c$ the particle will align with the flow at an angle called the Leslie angle [67]. In our case the threshold $\xi_c = \frac{3S+4}{9S}$ so assuming $S \approx S_{eq} = 1$ we get $\xi_c \approx 7/9$ [67].

The flow alignment parameter has not been widely studied although there are a couple of exceptions. On the experimental side, the flow alignment parameter has been calculated for the *Drosophila* wing epithelium [68] or mouse fibroblasts [69], revealing that ξ can have a range of values including negative. Flow alignment is generally included in theoretical studies, but investigation of the effect of the flow alignment remain few, with exploration of interplay between flow alignment and activity [70] and flow alignments effect on defect nucleation in active nematics with isotropic friction [67] as prominent exceptions.

2.3 Active nematics

While nematics are an equilibrium system, in using it to describe living systems, we want to describe the activity of the living constituents, exerting forces on their surroundings. This is often done by extending nematohydrodynamics by an active term to create *active nematics*. This term is added to the stress in the Navier-Stokes equations (14) as:

$$\Pi_{\text{active}} = -\zeta \mathbf{Q}. \tag{15}$$

The important difference to passive nematics is the constant energy injection, rendering the active nematic inherently out of equilibrium.

The field of active nematics was opened when Aditi Simha and Ramaswamy [43] discovered that active nematics are unstable to perturbations. For an active nematic with positive (negative) activity, any bend (splay) in the system, e.g. from fluctuations, will be unstable and be amplified [71]. The instability can be understood when we consider the force the particles exert (Figure 4). The active term may be

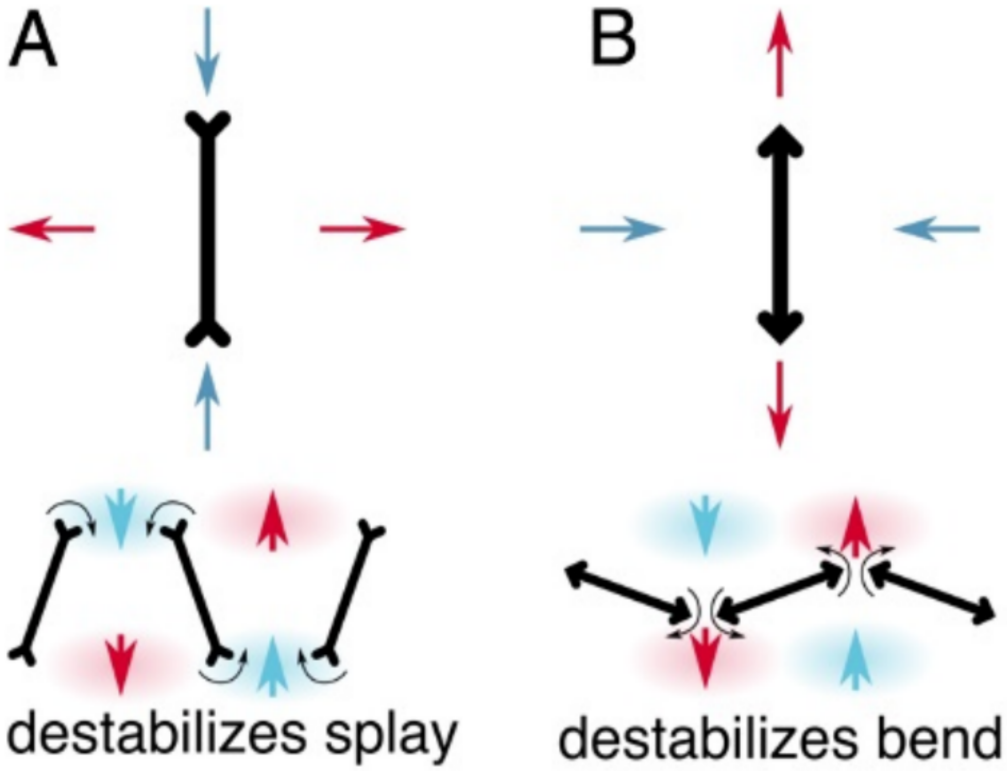

Figure 4: Contractile ($\zeta > 0$) (A) and extensile ($\zeta < 0$) (B) active particles. The flow field induced by the particles leads to instability to splay or bend. From [75].

understood as a force dipole term. A contractile particle, a so-called "puller", creates an inward flow in the direction of orientation and a perpendicular outward flow. Considering aligned particles, if we splay the alignment slightly, the inward flows of two neighbours will combine to create a torque towards each other as shown in Figure 4A. This means that a fluid of contractile active particles will be unstable to splay deformations. A similar effect leads to extensile particles, "pushers" with an opposite flow field, to be unstable to bend. These flow fields have been measured for the model organisms, the bacterium *E. coli*, a pusher, and the single celled algae *C. reinhardtii*, a puller [72–74].

When the activity is high enough, this instability will generate topological defect pairs in the nematic field, which are topologically protected features which can play a role in various systems. This phase is often called *active turbulence* [34, 76], different from classical, inertial, turbulence in its scaling laws and absence of energy cascade [77]. Active turbulence has also been proposed to be in its own universality class [78]. Note that active turbulence does not necessarily include topological defects and that the defect stirring phase can also be called defect chaos.

Active nematics have been widely studied and have been used to explain various

biological systems [2, 18, 30]. Although we are mostly interested in cellular systems, for which active nematics can be a good model, there are also synthetic systems which are certainly active nematics as they have been engineered as such [18]. The general setup for these synthetic active nematics, is a long filament, supplying the nematic order, and a molecular motor which walks on the filament, supplying the activity. In fact, two motors are coupled so that when each motor walks on a different filament, the filaments move against each other. The main classes are microtubule-kinesin or actin-myosin systems, with the microtubule system being the first [4]. These systems made it possible to study active nematics experimentally, verifying a decade of theoretical research.

2.4 Topological defects

Having mentioned the emergence of topological defects in active nematics, an exposition of topological defects, their nucleation, proliferation and the role they play in biophysics, is in order.

Topological defects are singularities in the orientation field. The name arises because they cannot be removed by smooth operations on the director field. Topological defects are characterised by their topological charge. The topological charge can be determined by going in a loop (called Burgers circuit) Λ around the defect and measuring the change in the orientation [20]:

$$\oint_{\Gamma} d\theta = k2\pi, \quad k \in \mathbb{Z}/2. \tag{16}$$

The Burgers circuit is illustrated in Figure 5**A**. Due to the two fold symmetry of the nematic, k has the value of half of an integer. As a smaller absolute charge also means lower energy of the defect, $\pm 1/2$ defects are most common and are the subject of this thesis.

A central difference between $\pm 1/2$ defects is that the $+1/2$ defect has a polar symmetry in the director field, whereas the $-1/2$ defect has a three fold symmetric apolar pattern. When the defects exert forces, this difference sets the defects as the $+1/2$ defect becomes self propelled. This effect will be discussed in Section 2.4.2.

Due to the topological nature of the defects – they can only be removed by annihilating with another defect or reaching an unanchored boundary – they are long lifetime phenomena in nematics. As well as a long lifetime, the defects affect the nematic profoundly, organising themselves into rasters [67], effecting interesting flow fields in wet nematics [70, 79] and generating stress patterns which affect the nematic [10, 80]. This conjunction of persistence and extensive interaction with their environment makes topological defects such a rich phenomenon. Here, I will explain the origin of defects, look at their interaction with their environment and describe the *defect chaos* phase created by the defects.

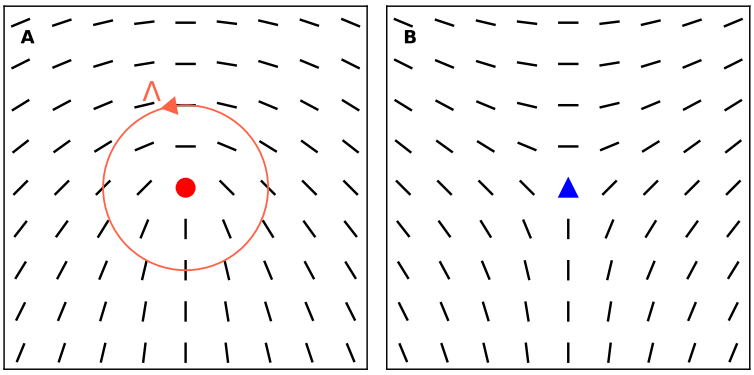

Figure 5: Topological defects of charge $+1/2$ (red circle, **A**) and $-1/2$ (blue triangle, **B**). Burgers circuit Λ in red (**A**) to quantify the defect charge. The polar (apolar) symmetry of the $+1/2$ ($-1/2$) defect is visible.

2.4.1 Defect generation

Defects can result from several sources. The simplest is confinement of the nematic, whereby the nematic is anchored to the boundaries which are chosen such that a loop along the boundary will result in some change of orientation which must be conserved over the nematic. Therefore a circular confinement results in topological charge $+1$, resulting in two $+1/2$ defects. Without anchoring, a nematic on a sphere has charge $+2$ (hairy ball theorem), resulting in four $+1/2$ defects [81].

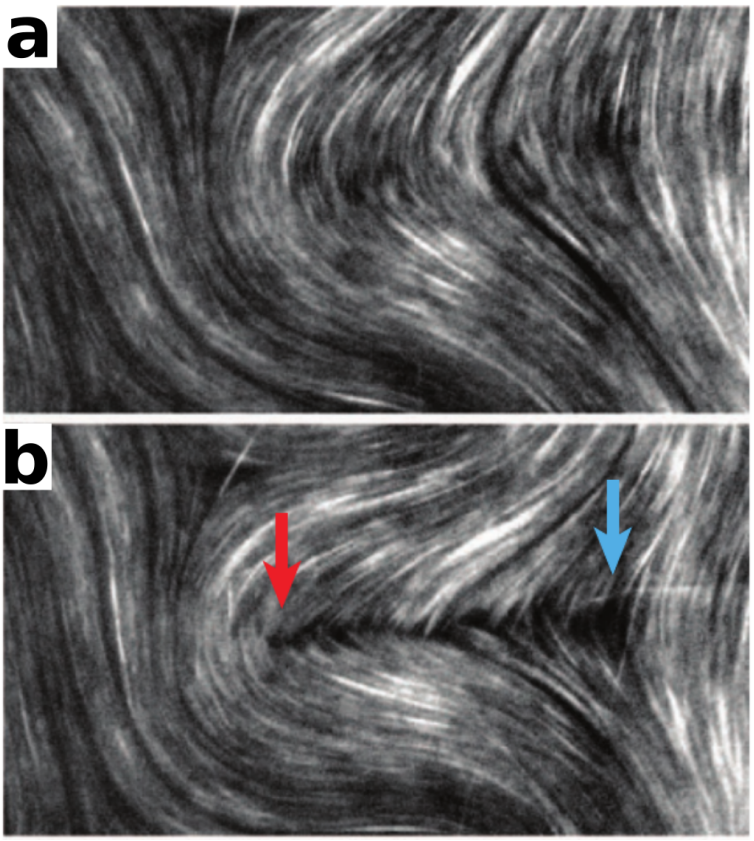

Figure 6: Nucleation and unbinding of a pair of $\pm 1/2$ defects in a Microtubule-Kinesin mixture. In **a** the bend instability is visible. In **b** the instability has grown to nucleate a pair of $\pm 1/2$ defects. In this case the system is extensile and so the $+1/2$ defect travels away from the $-1/2$ defect. From [4].

However, defects also appear in active nematics. Depending on the sign of the

activity, the active term destabilises either bend or splay deformations, leading to defect formation [34]. An active nematic with any noise in initial configuration or ongoing fluctuations will therefore produce defect pairs. In this case, pairs are produced, as the total topological charge cannot change as this would be energetically costly (infinitely in the limit [20]). This is illustrated well by the snapshots of an active extensile microtubule-kinesin mixture in Figure 6, from [4]. In Figure 6**a**, we see a bend in the material, this might occur due to fluctuations or because of other defects stirring up the director field. Then in Figure 6**b**, the bend region extends because it is unstable and nucleates a defect pair, $+1/2$ on the left and $-1/2$ on the right. The unbinding of one defect has a kind of catalytic effect because as the defect travels, it leaves behind a line of high distortion (which can dissipate in wet nematics) which is particularly favourable for defect generation [34].

Finally, defects in nematics may also be caused by the Berezinskii–Kosterlitz–Thouless (BKT) transition, which can be effected by temperature or density [21]. In the case of 2D nematics,the first order isotropic to nematic transition is not possible and the continuous BKT transition takes place. When the temperature is nonzero, defect pairs are nucleated all the time but mostly just annihilate. The BKT transition describes the transition to defect unbinding, destroying the nematic order. The defect appearance can be explained in a somewhat abridged manner as follows [20]. Taking the free energy as $F = U - TS$, a defect of core size a in a system of size R has a free energy contribution $F_{\text{def}} \sim \pi \ln(R/a)$ and an entropic contribution due to the free placement of the defect goes as $S \sim \ln[(R/a)^2]$. For the defect free energy contribution we find:

$$F_{\text{def}} \sim (\pi - 2T) \ln\left(\frac{R}{a}\right), \tag{17}$$

giving the critical temperature $T_{BKT} = \pi/2$, above which a free defect will lower the free energy.

In a 2 dimensional dry nematic, fluctuations (as effective temperature) is known to drive the Berezinskii–Kosterlitz–Thouless (BKT) transition, in which spontaneously generated defect pairs unbind to break the quasi long-range order of the nematic phase [20], as previously shown. During the BKT transition, defect pairs appear, which stay close at low temperatures, but unbind at higher temperatures and become randomly distributed [14]. This transition was shown for nematics analytically via renormalisation group analysis already in 1978 [21]. It has been observed in many systems, e.g. superfluid helium [20]. The BKT transition has been observed computationally for a nematic using a lattice model [22]. Also in a dry, freely moving particle model, with aspect ratios (related loosely to flow alignment parameter) the BKT transition has been observed [23, 24].

An analytical study of defect unbinding in active nematics found that low noise will stabilise the nematic phase by disrupting defect movement [26]. However, at higher noises, the BKT transition will still lead to the chaotic defect state, even at 0 activity [26]. Having seen that effective temperature leads to defect unbinding in

a passive nematic, the question then remains whether effective temperature plays a role in our systems of interest.

2.4.2 Defect characterisation

Defects in wet active nematics have characteristic flow and stress patterns, calculated from first principles and seen in experiments.

The flow around a defect has been calculated analytically by e.g. Giomi et al. [82] and has been widely observed experimentally [10, 40, 83] (Figure 7).

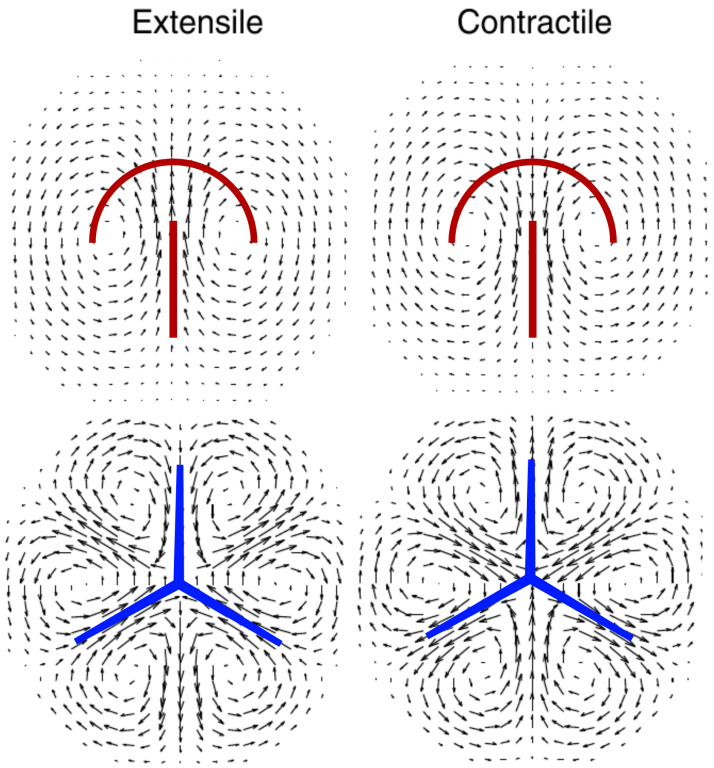

Figure 7: Flow of $+1/2$ (top) and $-1/2$ (bottom) defects for extensile and contractile active defects. The $+1/2$ defect has two counter rotating vortices, creating a net flow through the defect core. The $-1/2$ defect has 6 counter rotating vortices, resulting in no flow at the core. The contractile case is exactly the negative of the extensile case. From [18].

The $+1/2$ defect, owing to its polar symmetry, has a polar flow field comprised of two counter rotating vortices. This means that the $+1/2$ defect is self-propelled, a central feature to active nematics. The flow at the core is linear in the activity [82], meaning that a positive activity will result in positive core flow, propelled in the head direction, and negative activity will result in a negative core flow, in the tail direction. These defects are called extensile and contractile respectively. In fact, the direction of movement of the defects is a way of measuring whether a nematic is extensile or contractile. An extensile nematic functions via positive elastic stresses, whereas a contractile nematic has negative total elastic stress. A recent study was able to show how an individual contractile cell (pulling on its neighbours) is able to exert extensile stress (pushing on its neighbours) to make an extensile nematic, with the expected

defect movement [19].

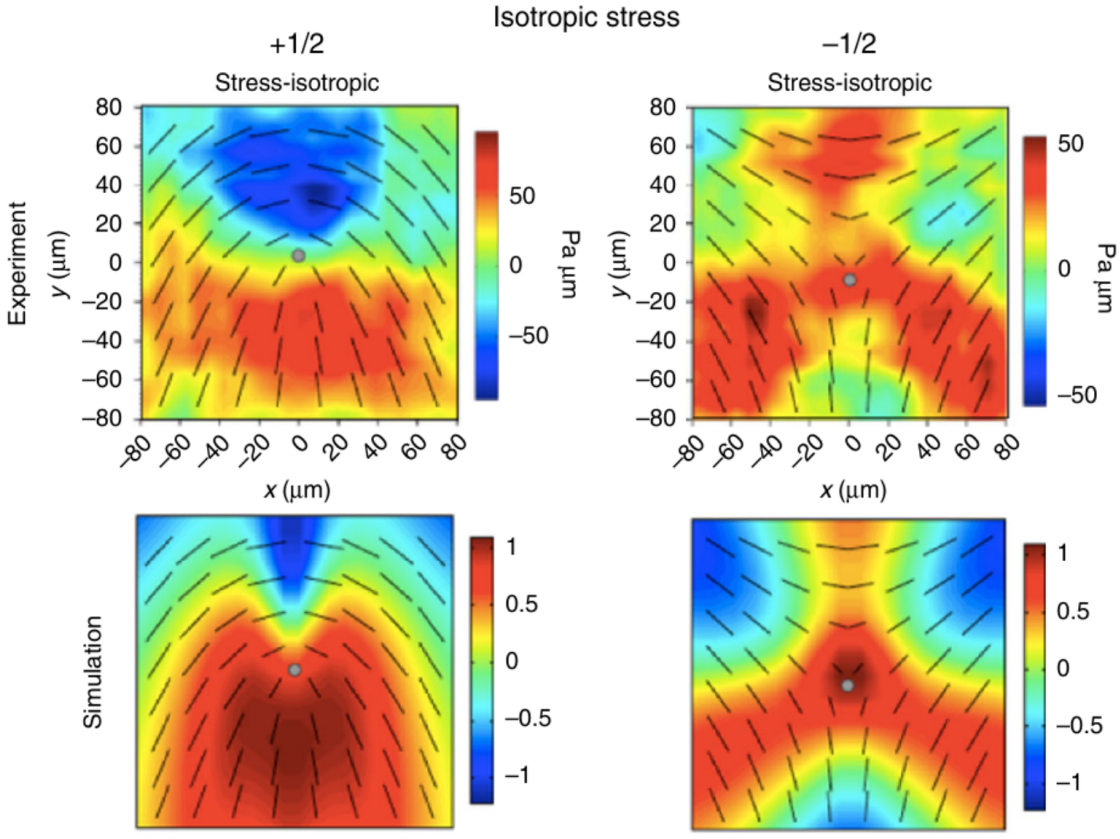

Figure 8: Isotropic stress patterns around $\pm 1/2$ extensile defects. A $+1/2$ defect has a dipolar pattern with compression at the head and tension at the tail. A $-1/2$ defect has a hexapole pattern. The top row has data from MDCK cells whereas the botton is from active nematics simulations. The simulations match the theory well. From [18].

The isotropic stress ($\sigma_{iso} = 1/2 \operatorname{Tr} \mathbf{\Pi}$) pattern around a defects follows the same polar-apolar pattern. While a $-1/2$ defect has a hexapole pattern, a $+1/2$ defect has a dipole stress pattern (Figure 8). The dipole changes its direction with the flow, so an extensile defect should have its negative pole at the defect head and vice versa. These stress patterns mean that defects are not just visual patterns in cell orientation but have a real effect on the mechanics of the cell layer.

2.4.3 Defect chaos

The self propelled $+1/2$ defects now move around, mixing up the nematic field. This creates a phase which has been called defect chaos [84], meso-scale turbulence [36] or active turbulence [34, 76, 85].

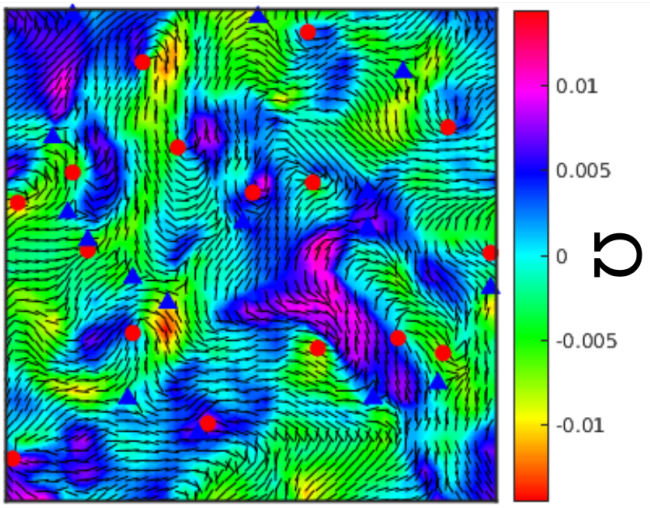

Figure 9: Snapshot of active turbulence from continuum simulations with director as black line and vorticity in colour. $\pm 1/2$ defects are marked with a red circle (blue triangle). Low turbulence jets are visible, as well as vortices.

This phase is characterised by a kind of gas of self-propelled $+1/2$ defects and diffusive $-1/2$ defects creating a swirling pattern full of jets and vortices. The flow correlation length is set by the defect density, which is is a power law in the activity [84].

An analysis of the active nematic as a coulomb gas found a phase boundary between the nematic phase and defect chaos as a function of activity and chaos [26].

In a very recent study, Krommydas, Carenza and Giomi [86] showed that a $+1/2$ defect in a passive nematic will be motile, if elasticity is taken into account. However they neglect the flow alignment, which turns out to be crucial in our results (Section 4.2.2).

3 Methods

I this section, we detail the equations of nematohydrodynamics, then explain the hybrid lattice Boltzmann simulation. This leads us to the definition of the two types of fluctuations. A table of the parameters used, their values and dimensions is presented (Table 1).

3.1 Nematohydrodynamics

We simulate the time evolution of the order parameter, $\mathbf{Q}$, and the velocity, $\vec{v}$. The evolution of $\mathbf{Q}$ depends on the molecular field, $\mathbf{H}$, as follows:

$$D\mathbf{Q} = \Gamma\mathbf{H}, \tag{18}$$

where Γ is the rotational viscosity and D is the co-moving, co-rotating derivative defined as:

$$D\mathbf{Q} = \partial_t\mathbf{Q} + \vec{v}\cdot\nabla\mathbf{Q} - \mathbf{S}. \tag{19}$$

The corotation term,

$$\begin{aligned}\mathbf{S} = &(\xi\mathbf{E} + \mathbf{\Omega})\cdot(\mathbf{Q} + \mathbf{I}/2) \\ &+ (\mathbf{Q} + \mathbf{I}/2)\cdot(\xi\mathbf{E} - \mathbf{\Omega}) \\ &- 2\xi(\mathbf{Q} + \mathbf{I}/2)(\mathbf{Q} : \nabla\mathbf{u}),\end{aligned} \tag{20}$$

accounts for the effect the flow has on the orientation of the particles. This is done by scaling the influence of the strain rate $\mathbf{E} = 1/2(\partial_i v_j + \partial_j v_i)$ vs the vorticity $\mathbf{\Omega} = 1/2(\partial_i v_j - \partial_j v_i)$ by the flow alignment parameter, ξ. The operator : is defined as $\mathbf{A} : \mathbf{B} = A_{ij}B_{ij}$

The flow is governed by incompressible Navier-Stokes equations with density ρ:

$$\rho(\partial_t\vec{v} + \vec{v}\cdot\nabla\vec{v}) = \nabla\cdot\mathbf{\Pi}, \quad \nabla\cdot\vec{v} = 0. \tag{21}$$

Here $\mathbf{\Pi}$ is the general stress tensor, a sum of pressure, viscose, elastic and active terms [18]:

$$\mathbf{\Pi}_{\text{viscose}} = 2\eta\mathbf{E}, \tag{22}$$

$$\begin{aligned}\mathbf{\Pi}_{\text{elastic}} = &-P\mathbf{I} + 2\xi(\mathbf{Q} + \mathbf{I}/2)(\mathbf{Q} : \mathbf{H}) \\ &- \xi\mathbf{H}\cdot(\mathbf{Q} + \mathbf{I}/2) - \xi(\mathbf{Q} + \mathbf{I}/2)\cdot\mathbf{H} \\ &- \nabla\mathbf{Q}\frac{\delta\mathcal{F}}{\delta\nabla\mathbf{Q}} + \mathbf{Q}\cdot\mathbf{H} - \mathbf{H}\cdot\mathbf{Q},\end{aligned} \tag{23}$$

$$\mathbf{\Pi}_{\text{active}} = -\zeta\mathbf{Q}. \tag{24}$$

3.2 Hybrid Lattice Boltzmann simulation

We employ a hybrid lattice Boltzmann approach, first described in Marenduzzo et al. [87] and since used widely in active nematics simulations [34, 88, 89].

This method entails solving the fluid flow (21) via lattice Boltzmann method and solving the nematic evolution (18) with a finite difference predictor corrector scheme with one correction step.

The lattice Boltzmann (LB) method is a mesoscopic simulation method where the lattice Boltzmann equation, a discretisation of the Boltzmann equation is solved [90]. Importantly, the Boltzmann equation can be shown to correspond to the Navier-Stokes equations.

We introduce the particle distribution function $f(\vec{x}, \vec{\xi}, t)$ which describes the density of particles in space $\vec{x}$ and velocity $\vec{\xi}$ at time t. At equilibrium, the distribution $f = f_{eq}$ is known as the Maxwell-Boltzmann distribution.

To obtain the evolution of the system we calculate the total differential df/dt:

$$\frac{df}{dt} = \left(\frac{\partial f}{\partial t}\right)\frac{dt}{dt} + \left(\frac{\partial f}{\partial x_i}\right)\frac{dx_i}{dt} + \left(\frac{\partial f}{\partial \vec{v}_i}\right)\frac{d\vec{v}_i}{dt} \tag{25}$$

$$\frac{\partial f}{\partial t} + \vec{v}_i\frac{\partial f}{\partial x_i} + \frac{F_i}{\rho}\frac{\partial f}{\partial \vec{v}_i} = \Omega(f) \tag{26}$$

with $d_t x_i = \vec{v}_i$ and $d_t \xi = F/\rho$. Equation (26) is called the Boltzmann equation. This is therefore a kind of continuity equation with the source term Ω on the right which is called the collision operator. On the left we see how f can change: advection with velocity, $\vec{v}$, and forces affecting the velocity with force density, F/ρ. The simplest and most widely used collision operator is called the BGK operator:

$$\Omega(f) = -\frac{1}{\tau}(f - f_{eq}) \tag{27}$$

named after Bhatnagar, Gross and Krook. The BGK operator implies exponential relaxation to the equilibium distribution f_{eq} with the characteristic time τ called the relaxation time.

To solve the Boltzmann equation on a lattice, it must be discretised. The discretisation is as follows (Figure 10): we define 9 possible velocities, with unit vectors $\vec{e}_i = (a, b); a, b \in \{-1, 0, 1\}, i \in 1...9$. $\vec{e}_1 = (0, 0)$ accounts for nonmoving particles, while the other $\vec{e}_i$ point to the neighbours (also diagonal) of the lattice site on the square lattice. This discretisation is called $D2Q9$ because we are in 2 dimensions and have 9 velocities. The velocities are weighted and we use the following weighting [60]:

$$\vec{w} = \left(\frac{4}{9}, \frac{1}{9}, \frac{1}{9}, \frac{1}{9}, \frac{1}{9}, \frac{1}{36}, \frac{1}{36}, \frac{1}{36}, \frac{1}{36}\right). \tag{28}$$

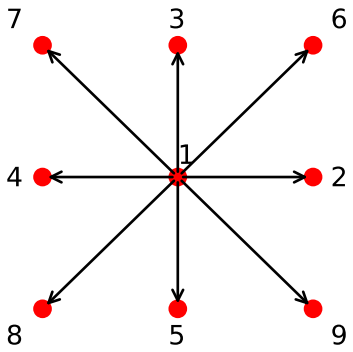

Figure 10: $D2Q9$ discretisation of velocities. There are now 9 possible directions ($\vec{e}_0 = (0, 0)$) in which particles can stream to neighbouring lattice points.

The weighting is necessary, so that moments are conserved [90].

The Boltzmann distribution function is now discretised so that t is discretised, $\vec{x}$ refers to a lattice point and $\vec{v}$ refers to the discretised velocities.

The step reads:

$$f_i(\vec{x} + \vec{c}_i\Delta t, t + \Delta t) = \tag{29}$$
$$f_i(\vec{x}, t) - \frac{\Delta t}{\tau}(f_i(\vec{x}, t) - f_i^{eq}(\vec{x}, t)),$$

using the BGK collision operator. The implementation proceeds in two steps. First, collision, in which the collision operator is applied:

$$f_i^*(\vec{x}, t) = f_i(\vec{x}, t) - \frac{\Delta t}{\tau}(f_i(\vec{x}, t) - f_i^{eq}(\vec{x}, t)). \tag{30}$$

The collision step simulates the equilibrating effect of collision. Following that, the streaming step, in which the particles move in their respective directions:

$$f_i(\vec{x} + \vec{c}_i\Delta t, t + \Delta t) = f_i^*(\vec{x}, t). \tag{31}$$

In this step, the components move in their relevant directions.

3.3 Fluctuation implementation

We implement fluctuations in the velocity and in the orientation.

3.3.1 Velocity fluctuations

Velocity fluctuations are implemented at the level of the Boltzmann equation as introduced in Adhikari et al. [91]:

$$f_i(\vec{x}+\vec{c}_i, t+1) = f_i(\vec{x}, t) + \frac{1}{\tau}\left(f_i^{\mathrm{eq}}(\vec{x}, t) - f_i(\vec{x}, t)\right) + \eta_i, \tag{32}$$

with fluctuations η_i. These fluctuations must conform to a fluctuation-dissipation relation which is done by a careful choice of η_i. The method was developed in [91, 92] and a detailed description can be found in [60] SI. We use one scalar, $u_{\kappa_B T}$, which sets the size of the fluctuations. The typical values are $u_{\kappa_B T} \in [0, 0.05]$.

These fluctuations can be understood as force fluctuations and as such, in a cell context, might be interpreted as extending and retracting focal adhesions as in [55]. A connection might also be drawn to fluctuating line tension in vertex or voronoi based models [56].

3.3.2 Initial noise on director

The system is initialised with some noise in the director field. This is done, because an active, non-fluctuating, nematic is metastable in the nematic state [34], so initial noise is needed to see the active turbulent phase.

The initial noise is implemented, for an initial angle θ_0, initial noise strength n_0 and uniform distribution U as follows:

$$\theta(t=0) = \theta_0 + n_0\, U[-\pi/2, \pi/2]. \tag{33}$$

3.3.3 Rotational fluctuations

Fluctuations in the orientation must be done carefully, so as not to break the constraints of symmetry and tracelessness on $\mathbf{Q}$. Considering $Q_{xx} = \cos 2\theta, Q_{yx} = \sin 2\theta$, choosing two random values and adding them to both components of Q does not exactly result in an angle change of the particle. We remedy this by calculating θ from $\mathbf{Q}$ and then adding a scaled random θ_r:

$$\theta_i(t+1) = \theta_i(t) + U[-\pi/2, \pi/2]\sqrt{\Gamma Q_{\kappa BT}}. \tag{34}$$

This way, we guarantee that the rotational fluctuations are physically plausible. Typical values are $Q_{\kappa_B T} \in [0, 0.05]$

The fluctuations in orientation take into account that the orientation of a cell is not necessarily exact and that even over small distances, i.e. within the nematic correlation length, orientations are not perfectly aligned but spread about a mean orientation as is visible in e.g. [93].

3.3.4 Effective temperatures

To make the comparison of fluctuation strengths with experiments possible, we define an effective temperature for velocity and rotational fluctuations. We define the effective temperature in units of the elastic constant K, which has the units of energy, justifying the name effective temperature.

The strength of velocity fluctuations are scaled by the ratio of viscous friction, η, to rotational diffusivity, Γ, along with density, η, and the nematic energy scale, C:

$$\hat{u}_{\kappa_B T} = \frac{T^u_{\text{eff}}}{K} = \frac{u_{\kappa_B T}}{(\eta/\Gamma\rho C)^{-3/2}} \frac{1}{K}. \tag{35}$$

The rotational fluctuation strength is scaled by the rotational diffusivity, Γ, and the density, ρ, as:

$$\hat{Q}_{\kappa_B T} = \frac{T^Q_{\text{eff}}}{K} = \frac{Q_{\kappa_B T}}{(\Gamma\rho)} \frac{1}{K}. \tag{36}$$

When we deviate from the single elastic constant approximation using K, we have two elastic constants k_1 and k_3. We then scale the effective temperatures by the average of the elastic constants as:

$$\hat{u}_{\kappa_B T} = \frac{2T^u_{\text{eff}}}{k_1 + k_3}, \quad \hat{Q}_{\kappa_B T} = \frac{2T^Q_{\text{eff}}}{k_1 + k_3} \tag{37}$$

3.4 Data analysis

A large part of this work relies on obtaining the average properties of defects. This is done with custom `matlab` code. From velocity and orientation data output from the hybrid lattice Boltzmann, we calculate the winding number at each point to get a topological charge field. The defects are then found using a breadth first search and the angle is calculated according to [94]. Aligning the defects by centre and angle, we can calculate average flow or stress fields over all defects from one simulation. From these average fields we can then calculate derivative quantities.

Table 1: Simulation parameters with name, symbol and value (or range) and dimension where length: L, mass: M and time: T.

Name	Symbol	Value	Dimension
Flow-alignment	ξ	$[-1, 1]$	1
Rotational diffusivity	Γ	0.05	T/M
Solvent viscosity	η	1/6	M/T
Density	ρ	40	M/L^2
Coupling parameter	C	1	M/T^2
Frank elastic constant	K	$[0.01, 0.05]$	ML^2/T^2
Splay elastic constant	k_1	$[0.01, 0.05]$	ML^2/T^2
Bend elastic constant	k_3	$[0.01, 0.05]$	ML^2/T^2
LB Relaxation time	τ_{LB}	1	T
Activity	ζ	0	M/T^2
Initial noise in alignment	n_0	0.05	1
velocity fluctuation	$u_{\kappa_B T}$	$[0, 0.05]$	ML/T^2
director fluctuation	$Q_{\kappa_B T}$	$[0, 0.05]$	M/T^3
Box edge length	L	256	L
LB timestep	τ	1	T
Simulation length	n_{steps}	$[20000, 30000]$	1

4 Fluctuations induce motile defects

Defect unbinding is known to result from fluctuations during the BKT transition in dry nematics. In this work however, we found that in a wet nematic, the fluctuation nucleated defects can unbind and become self propelled due to backflow effects. This is interesting because in real world systems fluctuations will always be present and indicates that activity is not necessarily needed for many effects that are ascribed to active nematics.

We therefore investigated the fluctuation-induced defects. I will first show general aspects of fluctuation generated defects and then go into the effects of individual parameters. We will further see that mixing fluctuations and activity can have interesting effects.

To make the results for force fluctuations and director fluctuations comparable, we keep the parameters the same, where they are not explicitly being varied. The normal values are: $u_{\kappa_B T} = 0.05, Q_{\kappa_B T} = 0.014, \xi = 1, K = 0.05$ leading to rescaled fluctuation strengths $\hat{u}_{\kappa_B T} = 0.024, \hat{Q}_{\kappa_B T} = 0.14$. The fluctuation strengths were chosen because they lead to the same defect density, while being deep enough into the defect chaos phase. They are furthermore justified by a comparison with experimentally measured fluctuation strengths.

4.1 Exploration of motile defects

We begin with an exposition of the defects, moving from a general picture to specific characteristics.

4.1.1 Defect chaos

Adding fluctuations to a passive nematic, we see a defect chaos phase for both force fluctuations ($\hat{u}_{\kappa_B T}$) and director fluctuations ($\hat{Q}_{\kappa_B T}$) (Figure 11). $\pm 1/2$ defects are spread throughout the simulation box, with aligned areas separated by bend walls. The evolution looks similar to extensile active nematics in the defect chaos / mesoscopic turbulence phase [34, 95] (See movies at [96]). Specifically, we see defect pair nucleation, followed by unbinding due to the self propelled movement of the $+1/2$ defect and slower, diffusive, movement of the $-1/2$ defect and annihilation. To highlight this we have drawn the focus to a pair nucleated in the first snapshot. While the $-1/2$ defect moves very little, the $+1/2$ defect escapes and moves far away. We also see the annihilation of the $\pm 1/2$ defect pairs for both rotational and force fluctuations.

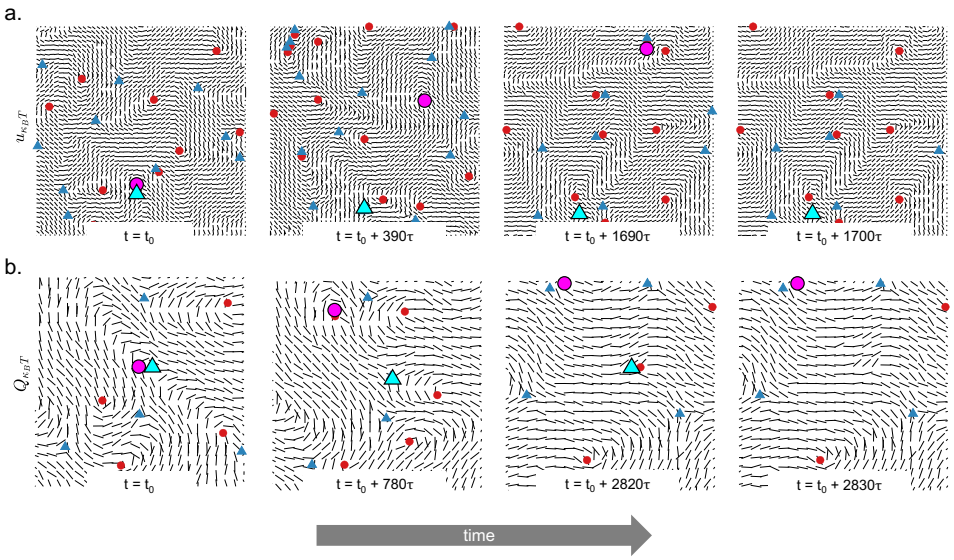

Figure 11: Timeseries of nematic evolution for (a) force $\hat{u}_{\kappa_B T} = 0.024, \xi = 1$ and (b) director fluctuations $\hat{Q}_{\kappa_B T} = 0.14, \xi = 1$. In both cases, we see nucleation of a defect pair, then the self propelled $+1/2$ defect escaping and travelling out of frame, while the $-1/2$ defect moves much slower. From the third to the fourth timepoints we can even see annihilation events; in the third panel a $+1/2$ and a $-1/2$ defect get very close and in the fourth panel they have annihilaited, leaving only a small disturbance in the director field. The direction of the movement of the $+1/2$ defect indicates that the system is extensile.

4.1.2 Trajectories

To highlight the defect movement and show the difference between $+1/2$ and $-1/2$ defect movement, we plot the trajectories of the defects (Figure 12). We see that whereas the $+1/2$ defect traces an extended trajectory with a high persistence length, the $-1/2$ defect moves very little in the same time showing a diffusive trajectory already at short times. Note that the trajectories look very similar for both fluctuations in orientation and velocity.

Qualitatively, this phase looks very much like the extensile active nematic defect chaos phase. This is surprising because in active nematics literature, the assumption is that the activity leads to the self propulsion of the defect and therefore the defect chaos phase [82]. However, here we are seeing the same behaviour for fluctuations only.

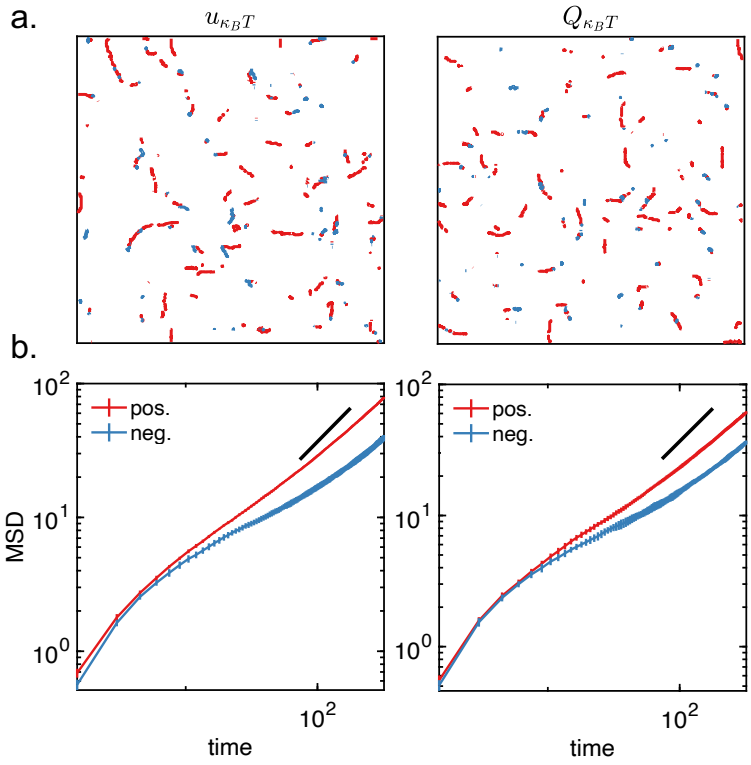

Figure 12: Defect movement. (a) Trajectories of $\pm 1/2$ defects (red and blue) and (b) MSD of defect movement. Left column shows force fluctuations $\hat{u}_{\kappa_B T} = 0.024, \xi = 1$, right column shows director fluctuations $\hat{Q}_{\kappa_B T} = 0.14, \xi = 1$. For both fluctuation types, $+1/2$ defects move faster at medium times but both $\pm 1/2$ defects end up being diffusive. From [60].

To analyse whether the movement of the defects is diffusive, we plot the mean squared displacement (MSD). For a defect with position $\vec{x}_t$ at time t, the MSD for an ensemble of defects is defined as:

$$\mathrm{MSD}(t) = \langle (\vec{x}_t - \vec{x}_0)^2 \rangle_{\mathrm{defects}}. \tag{38}$$

For diffusive movement, $MSD(t)$ is linear at long times. In our case we calculate separate MSDs for $\pm 1/2$ defects to see the difference in movement (Figure 12). We see that at short times, both $+1/2$ and $-1/2$ defects have the same MSD. However

in the medium term, $-1/2$ defects are slower. At long times, both MSD curves have the same slope, meaning that both types of defects are now moving in a similar way.

The explanation is as follows. In the short term, the defects are not yet unbound. In the medium term, the $+1/2$ defect is freely self propelling, while the $-1/2$ defect is just diffusing. However, in the long time, the defects act as gas particles and the movement becomes diffusive even for the $+1/2$ defect. At this point the slopes are the same, but the freely moving history of the $+1/2$ defect is represented by the offset between the MSD lines.

The long term diffusive movement for both defects is in line with data from human bronchial cells [44], which found the same diffusive movement for both defects. This is in contrast with data from bacteria [42], which see $+1/2$ defects moving faster throughout the measurement time, although this may be an effect of short measurement time or low defect density. As the bacteria are self-propelled, inducing active behaviour, whereas the human bronchial cells are only hypothesised to be active based on collective behaviour, leaving open the possibility of fluctuation driven dynamics, this difference in defect movement might be a way to distinguish noisy passive nematics from active nematics.

4.1.3 Flow fields

Seeing that $+1/2$ defects are self-propelled we wanted to see if the flow field conforms with typical double counter rotating vortex defect flow fields as presented in Figure 7.

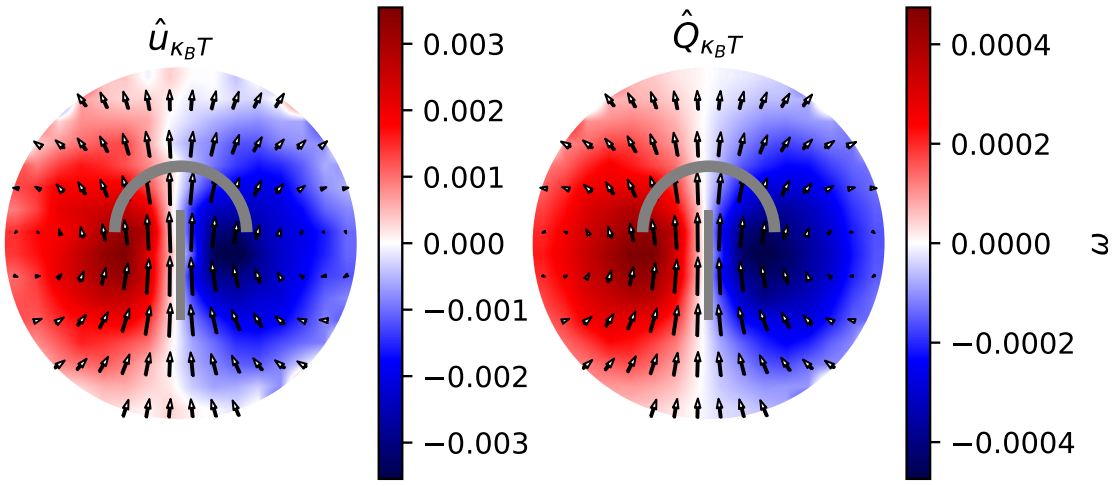

Figure 13: Flow fields of $+1/2$ defects. Both force fluctuations $\hat{u}_{\kappa_B T} = 0.04, \xi = 1$ and director fluctuations $\hat{Q}_{\kappa_B T} = 0.5, \xi = 1$ show the extensile active nematic defect flow of two counter rotating vortices, resulting in net flow at the defect core.

Indeed, the defects have the double counter rotating vortex flow field, resulting in

a jet at the defect core, with both having very similar patterns and vorticities (Figure 13). The pattern is very symmetric, with both vortices having similar strengths. This pattern matches those measured in passive nematics [83], cell layers [10, 42, 44] and predicted by continuum theories of active extensile nematics [70, 82].

4.1.4 Isotropic stress patterns

As mentioned in the introduction, the dipole isotropic stress pattern of the $+1/2$ defects has been found to be important for biological functions, e.g. lead to extrusion in MDCK layers [10]. Therefore, we next measure the average isotropic stress ($\sigma_{\text{iso}} = 1/2\,\text{Tr}(\mathbf{\Pi})$) around defects.

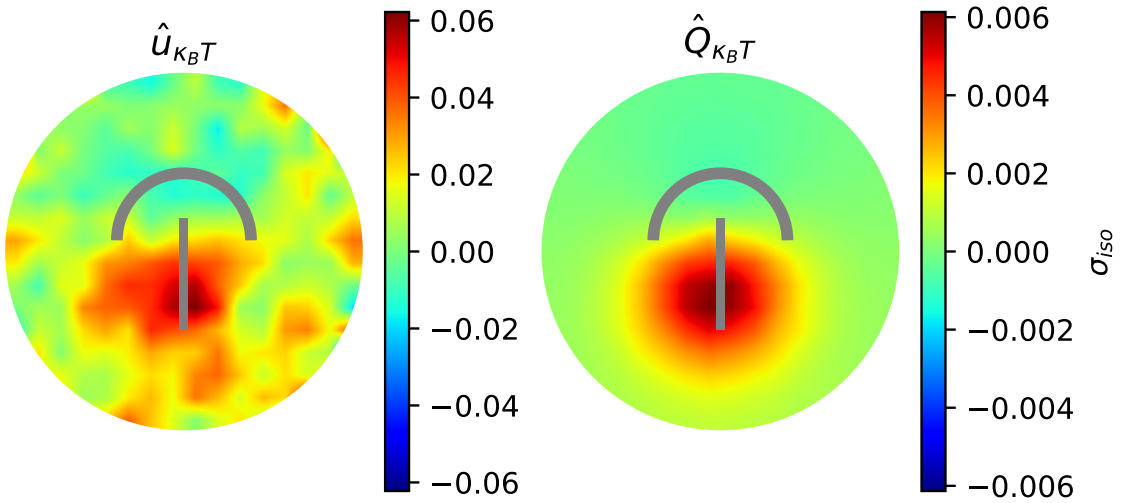

Figure 14: Isotropic stress patterns for $+1/2$ defects at $\hat{u}_{\kappa_B T} = 0.04, \xi = 1$ and $\hat{Q}_{\kappa_B T} = 0.5, \xi = 1$. The tension peak at the tail is consistent with active extensile nematics isotropic stress patterns, but we would expect to see compression at the head.

For both force and director fluctuations we see a dipole type pattern with compression at the head and tension at the tail (Figure 14). The magnitude of tension at the tail is higher than the magnitude of compression at the head. This is generally in line with the reported dipole pattern for a cell based simulation of an extensile active nematic [97] and the reported isotropic stress pattern for MDCK cells [10]. While the director fluctuation pattern is very clean, the force fluctuation pattern is not, even though both are averaged over a similar very large number of defects.

4.1.5 Conclusion

Our first analysis of the defects generated by fluctuations has shown that they are qualitatively very similar to those seen in active nematics simulations and to those seen in experiments. This is striking, as it calls into question the characterisation of biological tissues as active. In order to understand the defect generation, and its dependence on key parameters, we undertook a quantitative analysis of defect behaviour. In the next part, we look at the dependence of defect flow and stress fields on fluctuation strength and nematic-hydrodynamic coupling, called flow alignment.

4.2 Extensility depends on fluctuation strength and flow alignment

A key feature of active defects is the self propelled motion of the $+1/2$ defect. To quantify this effect and therefore allow comparison of active and fluctuation generated defects, we construct an *extensility parameter* (Figure 15). We orient the defect such that the head-tail axis is exactly the y-axis and the head is above the tail. To construct a measure of extensility which goes to 0 when the flow is isotropic and ± 1 when the flow is exclusively in the y direction (extensile or contractile, respectively), we define for the flow at the defect $\vec{U} = (U_x, U_y)$:

$$\mathcal{E} := \frac{\langle U_y \rangle}{\langle |\vec{U}| \rangle}. \tag{39}$$

Therefore, $\mathcal{E}$ goes from -1 for fully contractile defects, to 0 for no defect / passive defects, to 1 for extensile defects, as required.

The averaging is done over a square, concentric with the defect, of height and width 6 lattice Boltzmann units (Figure 15). This width was determined to be the smallest box size which was stable at low extensility.

4.2.1 Fluctuation strength

We first wanted to see the transition to self propelled defects so we vary both fluctuation strengths from 0 to deep into the defect chaos phase.

As the fluctuation strength increases, systems with force fluctuations, $\hat{u}_{\kappa_B T}$, and orientational fluctuations, $\hat{Q}_{\kappa_B T}$, transition very quickly to completely extensile defects (Figure 16). Note that when there are no defects, we set $\mathcal{E} = 0$ to make the transition visible in the plot. Although systems with force fluctuations and orientational fluctuations transition at different points and at different speeds, this is not relevant as they are not immediately comparable. Nevertheless, it is worth noting

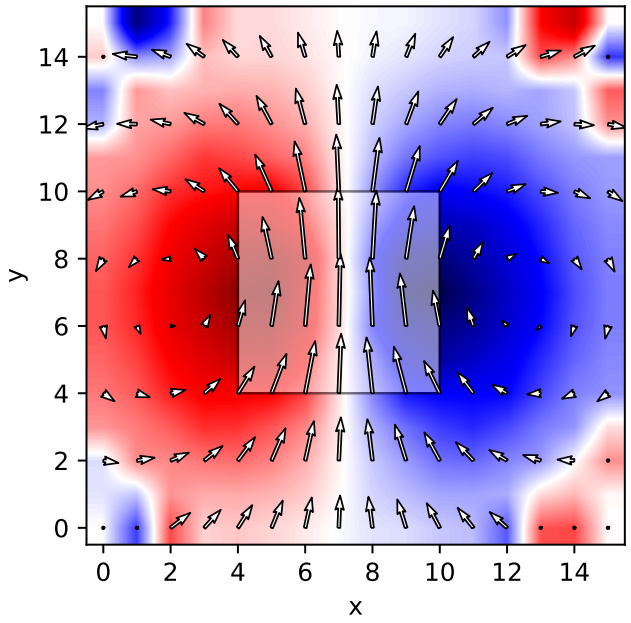

Figure 15: Calculation of extensility $\mathcal{E}$, in this case $\mathcal{E} = 0.98$. Velocity as quiver, vorticity in colour. We take the velocities in a 6×6 square around the centre of the defect. We take the largest box which captures the flow core – the box were larger, we would include velocities on the outside of the vortex, which are negative in the y direction.

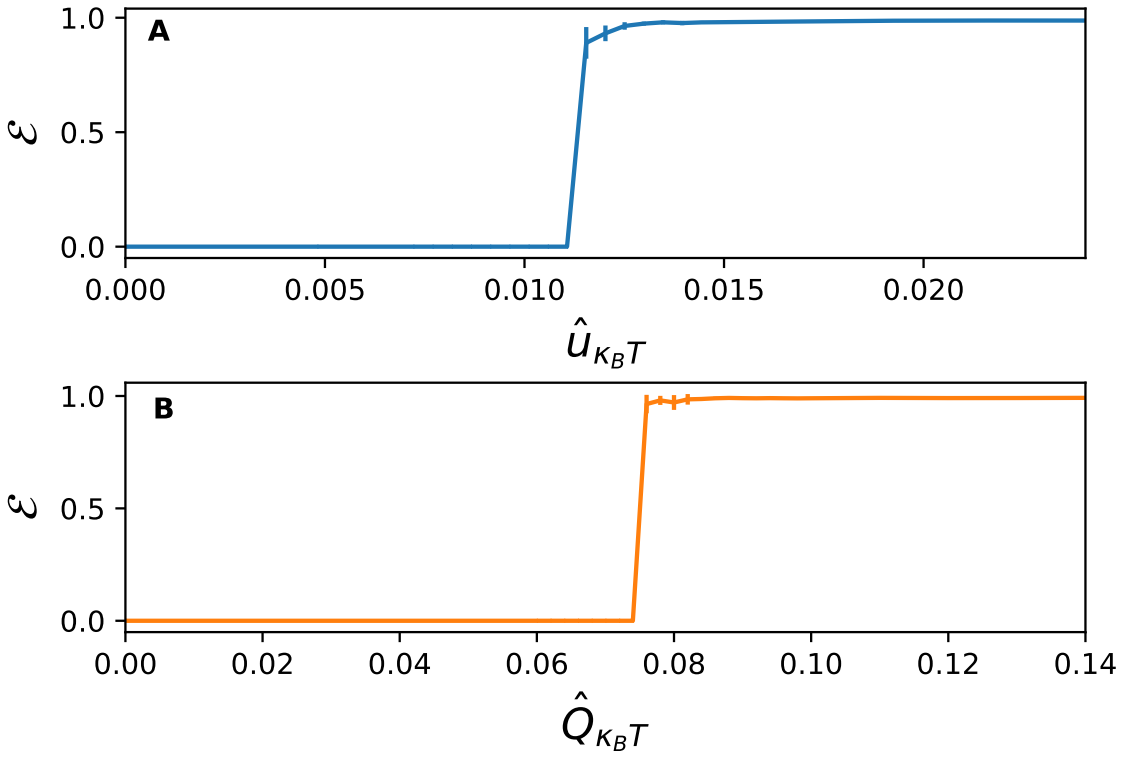

Figure 16: Extensility given by (39) (mean ± s.d.) of defects generated by force fluctuations (a) and director fluctuations (b) at $\xi = 1$. Both fluctuation types show an abrupt transition from $\mathcal{E} = 0$ to fully extensile, $\mathcal{E} = 1$, at the points where defects appear. The curves look like a step function, with no change in extensility over a large range of fluctuations.

that the transition is very abrupt – there are no half extensile defects. This may be explained by the life cycle of the defects – they must overcome the binding state to be counted for this value, which means that they must simply have a certain velocity / force. Combined with the fact that $\mathcal{E}$ is not sensitive to the magnitude of the flow / speed of the defects, it makes sense that we would see a step like shape. However, it does reveal that the defects must fully develop the jet at the core to unbind. This means that this is not BKT transition related, as there defects would unbind regardless of flow pattern. So we can be sure that after the transition the defects have the typical flow field shape. Further testing has shown that the velocity of the defect does not follow the same step shape.

4.2.2 Flow alignment

To investigate the remarkable effect a topological defect has on the flow, inducing a double vortex flow field, we investigate the parameter which tunes the interaction between nematic and fluid, the flow alignment parameter ξ. For natural systems, ξ has rarely been measured, but a study of *Drosophila* pupal wing epithelia and one on mouse fibroblasts concluded that ξ can take a range of values including negative values [68, 69]. Therefore, we scan the flow alignment $\xi \in [-1, 1]$ for various different scenarios to understand the flow alignment parameter and how its effect interacts with the effects of other parameters.

Scanning the flow alignment, ξ, for a single fluctuation strength in $\hat{u}_{\kappa_B T}$ or $\hat{Q}_{\kappa_B T}$ reveals that the value of the flow alignment parameter determines the sign and the magnitude of the extensility (Figure 17). We also see a saturation at $|\mathcal{E}| = 1$ when the flow alignment magnitude is high. At lower flow alignment, defects are not extensile or do not appear at all. This means that, at low fluctuation strengths, flow alignment is necessary for (motile) defect formation, setting these defects apart from BKT generated defects.

To investigate the saturation and the behaviour at low flow alignment we vary the fluctuation strength simultaneously with the flow alignment.

When varying fluctuation strength and flow alignment simultaneously, we see some interesting behaviour (Figures 18, 19). For lower fluctuation strengths, there is a $|\xi|_{\min}$ under which no defects appear. This suggests that at low fluctuation strengths, backflow effects are already at play in nucleation of defects. For higher fluctuation strengths, defects appear at all ξ, but are not extensile ($\mathcal{E} = 0$) if the flow alignment is too small. Here it seems the backflow is not necessary for all defect generation but still for extensility.

At very low $|\xi|$ but large fluctuation (e.g. Figure 19**B**, $\hat{u}_{\kappa_B T} = 0.024$), there is an interval on the flow alignment in which the defect density stays constant. Here, there are no defects for lower fluctuation strengths, but they appear with increasing

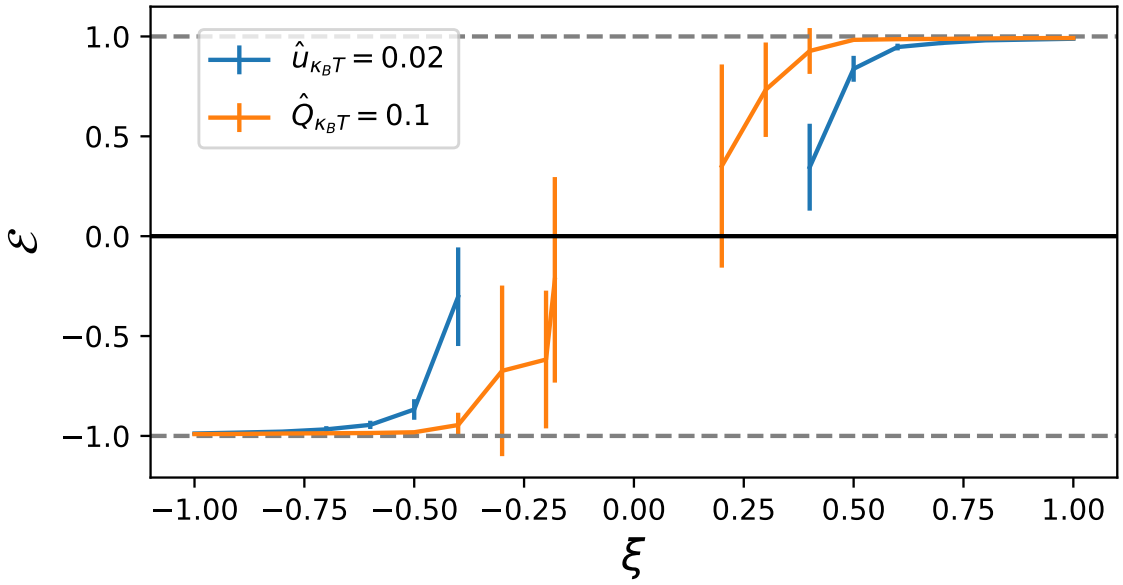

Figure 17: Extensility $\mathcal{E}$ given by (39) (mean ± s.d.) for $\hat{u}_{\kappa_B T} = 0.024$ and $\hat{Q}_{\kappa_B T} = 0.14$ for a range of flow alignment, $\xi \in [-1, 1]$. The sign of the flow alignment parameter determines the sign of the extensility. We see that extensility saturates at $|\mathcal{E}| = 1$ for high magnitude flow alignment. However, when $|\xi|$ is lower, the extensility goes down and for very low $|\xi|$, defects can disappear completely. Black line indicates extensility with no backflow. Dashed grey lines at ± 1 as guides for the eye.

strength of fluctuations. It seems that here we observe the BKT transition, the generation of non motile defects and that this is quite separate from the flow pattern formation. Further studies are required to investigate how the mechanisms of flow alignment assisted defect generation and BKT defect generation interact, if at all.

Furthermore, the defect density is strongly dependent on the flow alignment, ξ, with lower defect density at lower flow alignment (Figures 18**B**, 19**B**). At lower fluctuation strengths, the defect density, n_{def}, rises monotonically with the flow alignment, although it does show saturating behaviour as the flow alignment approaches $\xi = 1$. However, at higher fluctuation (e.g. $\hat{Q}_{\kappa_B T} = 0.4$), we find that n_{def} peaks at $|\xi| \approx 0.3$ and then decreases as the flow alignment magnitude increases. The cause of this effect is not clear.

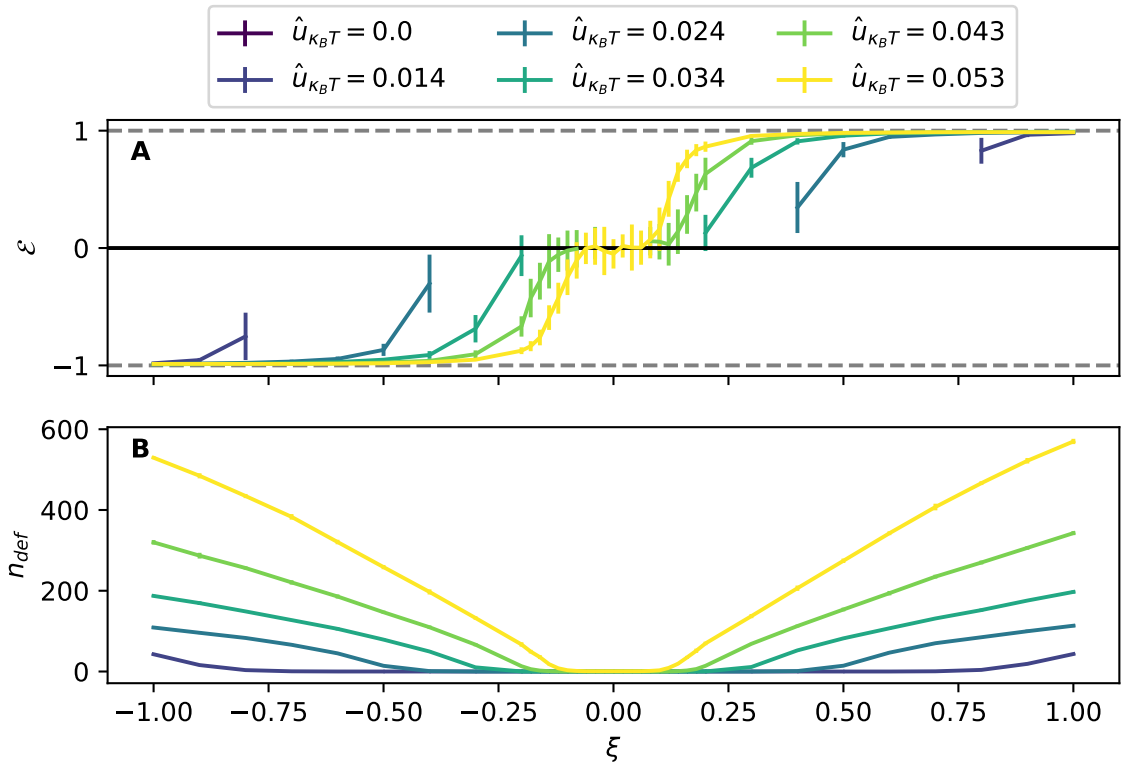

Figure 18: Varying velocity fluctuations $\hat{u}_{\kappa_B T}$ and flow alignment ξ. **A** shows the extensility $\mathcal{E}$. We see that at $\xi < 0$, $\mathcal{E} < 0$ and $\xi > 0$, $\mathcal{E} > 0$. While at low fluctuation strengths the defects are not generated at lower $|\xi|$, with increasing fluctuations, the transition becomes sharper, although $\mathcal{E}(\xi = 0) = 0$ holds. The black line represents the results for no backflow.
B shows the number of defects. We see that at lower fluctuation values, defects are only formed at higher $|\xi|$. However, as the fluctuations increase, defects can be generated at $\xi = 0$, however, they are not extensile. We also see that generally defect density increases with fluctuations.

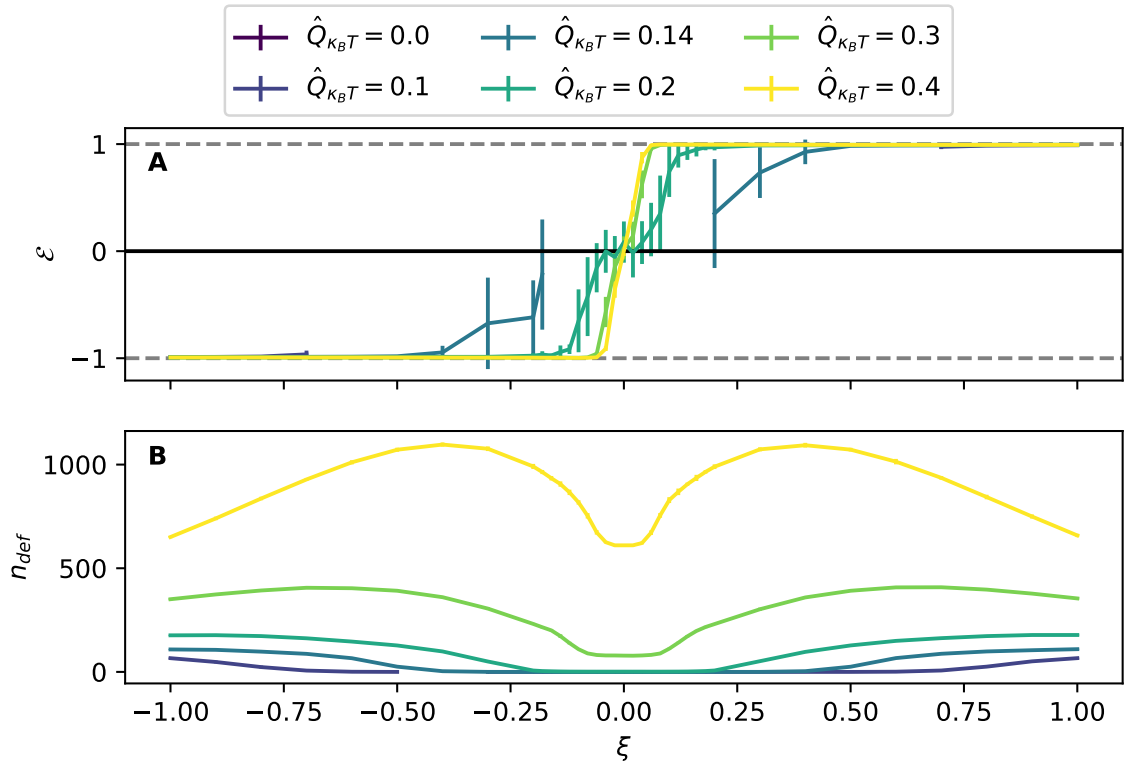

Figure 19: Varying velocity fluctuations $\hat{Q}_{\kappa_B T}$ and flow alignment ξ. **A** shows the extensility $\mathcal{E}$. We see that at $\xi < 0$, $\mathcal{E} < 0$ and $\xi > 0$, $\mathcal{E} > 0$. While at low fluctuation strengths the defects are not generated at lower $|\xi|$, with increasing fluctuations, the transition becomes sharper, although $\mathbf{E}(\xi = 0) = 0$ holds. The black line represents the results for no backflow.
B shows the number of defects. We see that at lower fluctuation values, defects are only formed at higher $|\xi|$. However, as the fluctuations increase, defects can be generated at $\xi = 0$, however, they are not extensile. We also see that generally defect density increases with fluctuations, although at high fluctuation strength and flow alignments, the number of defects decreases again.

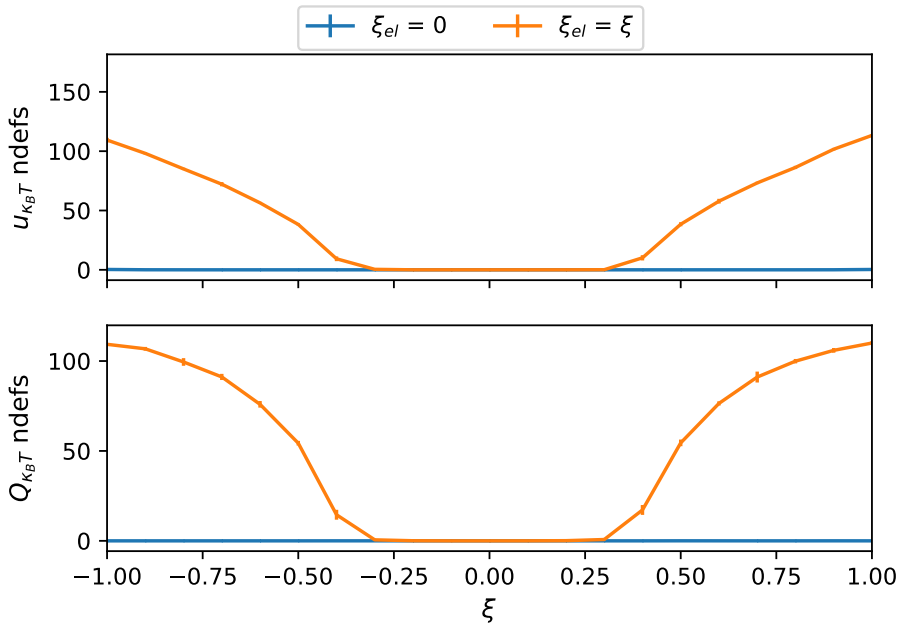

Figure 20: Non-BKT defect generation depends on elastic backflow, modulated by ξ_{el} Defect generation with elastic flow alignment parameter ξ_{el} the same value as the corotational flow alignment parameter $\xi_{el} = \xi_S$ or $\xi_{el} = 0$. $\hat{u}_{\kappa_B T} = 0.024, \hat{Q}_{\kappa_B T} = 0.14$

4.3 Backflow is necessary for motile defects

Backflow is the effect of nematic order on the hydrodynamics and vice versa. Simulating without backflow, we find that the defects are not extensile ($\mathcal{E} = 0$, Black line in Figure 17). This suggests that backflow is essential for extensile behaviour.

Because the flow alignment parameter, ξ, appears both in the corotation term $\mathbf{S}$ in the Beris-Edwards equation for $\mathbf{Q}$ evolution (Eq. 18) and in the flow alignment, specifically in the elastic stress term of the Navier-Stokes equations (Eq. 21), we split the term into corotational ξ_S and elastic ξ_{el}. This allowed us to isolate the effects of each, and we found that the defect generation depends on the elastic ξ_{el}, rather than ξ_S in the corotation term, confirming that it is the elastic behaviour which leads to extensile defects (Figure 20). This defect generation is at effective temperatures below those at which defects are generated even at no flow alignment $\xi = 0$, meaning that these are not BKT defects.

Following the investigation of fluctuation strength, effect of flow alignment and backflow, we observe a behaviour where fluctuations nucleate defects and if the backflow is high enough, a flow field develops that will unbind the defects leading to the defect chaos phase. The flow alignment parameter plays a twofold role: at low fluctuation strength, a high flow alignment can lead to the formation and unbinding of extensile defects (Figure 17). On the other hand, at high fluctuation strengths, even

if the flow alignment is low, defects might nucleate but will not become extensile.

4.4 Interaction of fluctuations and activity

Having seen that fluctuations can have an extensile or contractile effect, depending on the flow alignment, we wanted to explore what happens when we combine activity, a form of active stress generation, and fluctuations. Both can have an extensile or contractile effect, so we check how these effects interact.

Calculating the extensility for various values of rotational fluctuations and activity at a positive flow alignment ($\xi = 1$), depending on the strength of each, we see either full extensility or contractility ($\mathcal{E} = \pm 1$). This means that at most parameter values, either activity or fluctuations dominate (Figure 21). When there are no fluctuations (bottom row), we see the expected behaviour (see Section 2.3) of contractile defects (blue) at negative activity, $\zeta < 0$, and extensile defects (red) at positive activity, $\zeta > 0$. In the same way, when there is no activity, $\zeta = 0$, (middle column) we see the expected transition from no defects to very extensile defects as the fluctuation strength increases (as in Figure 16).

However, off these axes we see interesting behaviour. First, the extensility is not symmetric about $\zeta = 0$. This is because $Q_{\kappa_B T}, \xi = 1$ has an extensile effect at any magnitude. However, we see that for high negative activity, low fluctuation strengths are dominated by the activity and we get contractile defects, whereas high fluctuation strengths still dominate activity to make an extensile defect. At $\hat{Q}_{\kappa_B T} = 0.08, \zeta = 0$, we see defects and at $\hat{Q}_{\kappa_B T} = 0, \zeta = -0.01$ the activity is not strong enough to create defects. When $\hat{Q}_{\kappa_B T} = 0.08, \zeta = -0.01$ (b in Figure 21), there are no defects, so it seems that although the activity is not strong enough to nucleate defects, it is strong enough to counteract the fluctuations and suppress defect formation. In this way, the fluctuations with positive flow alignment and negative activity cancel each other out.

Simulating the same parameter set, except with $\xi = -1$ we see an inverted pattern of contractile defects in the upper left triangle and only extensile defects for high activity and low fluctuation strength (unpictured).

From the figure we see that, if we have a system at $\hat{Q}_{\kappa_B T} = 0.1$ and $\zeta = -0.05$ (a in Figure 21) and lower the activity magnitude (step to the right), we can switch contractile to extensile. The same holds for starting at the same point but increasing the fluctuation strength (step upwards). In this way a cell layer could switch from extensile to contractile or vice versa by tuning only one of activity or fluctuation strength.

In Balasubramaniam et al. [19], defects became contractile after an E-cadherin knockout decreased active inter-cellular tension. It is entirely plausible that reduced inter-cellular tension might lead to more cell shape fluctuation. This experiment could

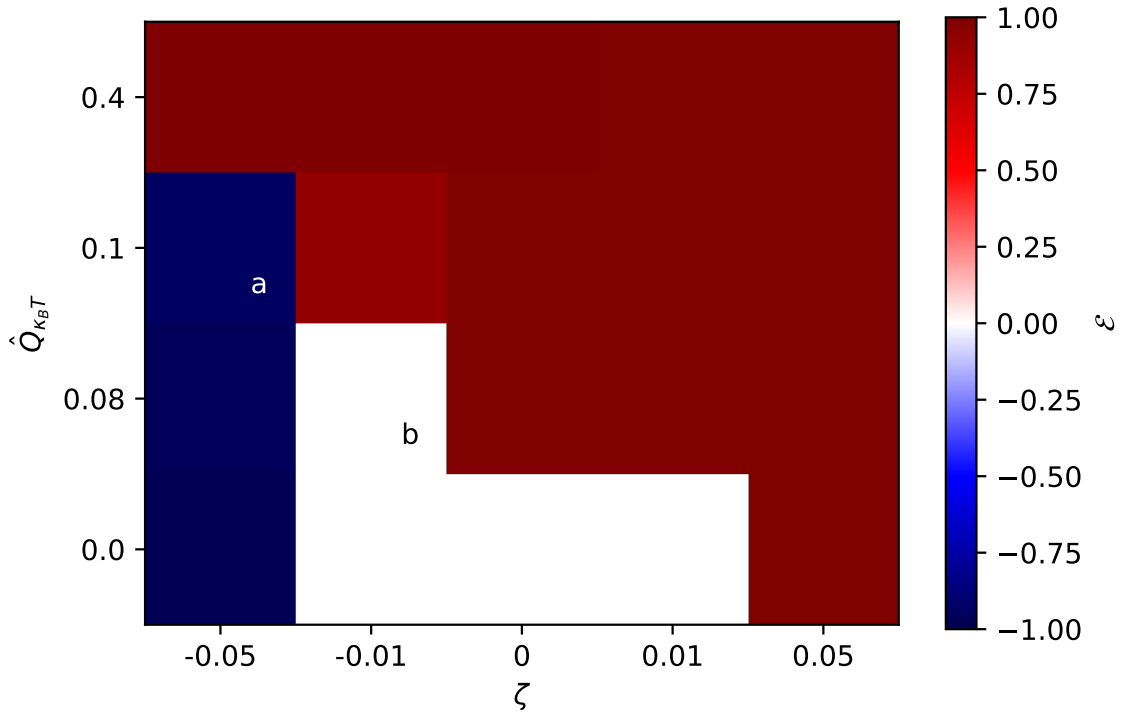

Figure 21: Rotational fluctuations with positive flow alignment have an extensile effect, which can be stronger than activity. Extensility $\mathcal{E}$ defined (39) of $\hat{Q}_{\kappa_B T}$ vs ζ at $\xi = 1$. Behaviour at $Q_{\kappa_B T} = 0$ and $\zeta = 0$ as expected. When both activity and fluctuations are present, the effects mix. At low fluctuation strength and activity ($\hat{Q}_{\kappa_B T} = 0.08, \zeta = -0.01$, (b)) they cancel each other out and no defects are generated.

therefore be explained by a noisy active nematic, where the activity is reduced.

4.5 Discussion of fluctuation strength

Having shown that fluctuations can generate extensile defects and suggested that real cell systems may be driven in this way, it is important to look at the fluctuations and judge whether they reflect fluctuations that have been experimentally observed.

Fluctuations in the orientation of the cells can be contextualised in several different ways. A recent study on *Drosophila* embryo wings clearly showed the fluctuations in orientation [93]. Taken from an aligned patch, a histogram of the orientations showed a gaussian like distribution with a surprisingly wide standard deviation of 0.38 radians.

Let us first consider the estimation of effective temperature from topological defect orientations in confined fibroblast cells [11], where the authors found an effective temperature $0.1 < T_{\text{eff}}/K < 0.2$, where K is the Frank elastic constant. The authors concluded that in this system activity contribution to the defect dynamics is small (see Fig. 4g of [11]). In their context T_{eff}/K is dimensionless. With $Q_{\kappa_B T} = 0.014, \Gamma = 0.05, \rho = 0.04$, $\hat{Q}_{\kappa_B T} = 0.14$ which is in line with the estimated values for the fibroblasts in [11]. Note that this is just an example value, and the minimum fluctuation level needed in our simulations to nucleate defects is even smaller.

A more direct comparison was recently made possible with measurements of the rotational diffusion constant of rat embryo fibroblasts [58]. The authors model the rotation of cells on a periodically stretched medium with a Langevin equation including a forcing term and a random diffusive term. This is actually very similar to our fluctuation implementation. The authors found a fluctuation strength as $\sqrt{2D} \in [\sqrt{10^{-5}}, \sqrt{10^{-3}}]$ corresponding well to our range $\sqrt{\Gamma Q_{\kappa_B T}} \in [\sqrt{10^{-5}}, \sqrt{10^{-3}}]$ for $Q_{\kappa_B T} \in [0.008, 0.1]$ which corresponds to effective temperatures of $Q_{\kappa_B T} \in [0.08, 1]$.

Finally, a timescale comparison shows that even in active systems, fluctuations may play a role. The active timescale in active nematics goes as $\tau_a = \eta/\zeta$ and from studies in MDCK cells [10] can be estimated as $\tau_a \approx O(10^2)$. For orientational fluctuations, the timescale is $\tau_Q = (\Gamma Q_{\kappa_B T})^{-1/2} \approx O(10^2)$, so of the same order. As the activity and fluctuations vary in different tissues, the importance of each may vary. However, in this case the timescales are very similar and may allow for interplay of activity and fluctuations as we have seen throughout this work.

The hydrodynamic fluctuations introduced in our model, u_{kBT}, appear as a source term in the momentum equation and as such correspond to fluctuations in the traction forces. The fluctuating forces that cells exert on their surroundings have been extensively documented [53, 56, 98] and are associated to various sources including,

but not limited to, traction force fluctuations exerted by focal adhesions [54, 55, 99], association/dissociation of stress fibres [100], and oscillations in Rho proteins [101, 102]. The amplitude of the fluctuations have been shown to reach values as high as 50% [55] in mouse embryo fibroblasts and even 10 fold change in keratinocytes [54]. Importantly, these fluctuating forces are persistent and quite regular, justifying continual addition of hydrodynamic fluctuations in our model. Considering the effective temperature of the hydrodynamic fluctuations, $\hat{u}_{\kappa_B T}$, as used throughout, a medium velocity fluctuation strength such as $u_{\kappa_B T} = 0.05$ results in an effective temperature $\hat{u}_{\kappa_B T} = 0.02$. This is far below temperatures estimated in the fibroblast study mentioned earlier [11].

Together, these different estimates show that the fluctuation levels that give rise to defect nucleation in the continuum model are well below the range estimated in the various experiments. This is not surprising since cell scale fluctuations, in the cell shape, cell area, cell alignment, and in the traction forces are typically visible in experiments of the cell monolayers. We emphasise that in our model the motile defects are seen over a wide range of fluctuations and for different implementations of fluctuations in the model, and thus represent a robust feature of the system.

Another way to test the plausibility of our results is by comparing to results from active simulations (Figure 22). Although we are not comparing directly to experiments, if the fluctuations results match the activity results, the fluctuations results have the same explanatory power for systems in which active nematics was used to explain the results. It is evident that the same velocity scales are obtained in both cases, further reinforcing the idea that fluctuation-induced features of the defects can reflect those obtained from the activity (Figure 22).

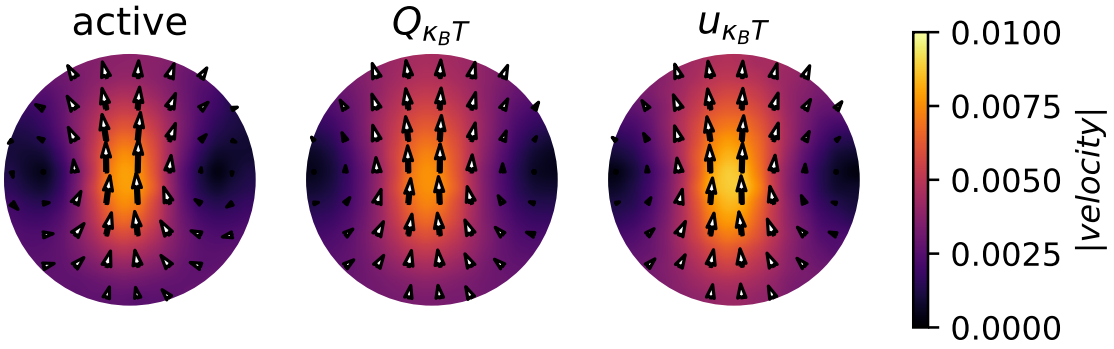

Figure 22: Comparison of flow between activity $\alpha = 0.045$, director fluctuations $\hat{Q}_{\kappa_B T} = 0.17$ and force fluctuations $\hat{u}_{\kappa_B T} = 0.03$ with $\xi = 1, K = 0.05$. These values were chosen to match in defect density. The patterns are very similar in shape and magnitude.

We additionally note that using estimates of the strain rates of $\sim O(10^{-2} hr^{-1})$ from experiments [10], and the correlation length of $\sim O(100\mu m)$ [19], and comparing them with the characteristic strain rates $\sim O(10^{-4})$ and correlation lengths $\sim O(10^{1})$

in simulation units, the velocities obtained in simulation units can be mapped to $\sim O(\mu/hr)$ in the physical units, that is comparable to the averaged velocities around topological defects that are observed in the experiments [10, 19].

In this regard, it is also important to note that the activity level can change across different cell types and even in the same tissue at different stages. For example, fibroblasts are believed to be very weakly active [11], and could be more strongly affected by fluctuations. Similarly, the activity levels are strongly reduced as the cells within a confluent tissue approach a glassy state, where again activity levels are significantly reduced and fluctuations can play a dominant role [103].

4.6 Summary

In this Chapter, we have shown that fluctuations in velocity or orientation can lead to a defect chaos phase including self-propelled $+1/2$ defects. We investigated the effect of fluctuation strength and flow alignment on defect formation and unbinding. This led us to an understanding of the defect formation as follows: fluctuations continually nucleates defect pairs; when the $+1/2$ defect interacts with the flow, it develops a polar flow pattern which means that the defect is self propelled. This force leads to defect unbinding and therefore the defect chaos phase. Switching off the backflow definitively showed that the coupling between flow and nematic is necessary for the phenomenon. Adding activity, we saw that fluctuations and activity can work with or against each other, meaning that a change in fluctuation strength or activity can switch the direction of $+1/2$ defect movement. Finally, a thorough comparison to available experimental fluctuation data showed that the both fluctuation strengths in our model are realistic and the resultant dynamics match those seen in experiments.

5 Elasticity determines defect traits

The usual single elastic constant approximation, as used in the first part of this thesis, is clearly reductive and hides a rich phenomenology of e.g. defect shape or density [5, 104]. The effect of differing bend and splay elastic constants in active nematics was explored by Zhang et al. [5] experimentally and computationally. Using an F-Actin based system, they varied k_1 and k_3 by adding microtubules, thereby increasing the bend constant. They found that the defect shape is affected very strongly, with V shaped defects when $k_3 > k_1$ and U shaped defects when when $k_1 > k_3$ (Figure 23). A molecular dynamics study by Joshi et al. [104], varied an activity renormalised filament stiffness, a parameter which corresponded well to the persistence length of the filament. As well as finding the V and U shapes at the stiffness extremes, they find scaling laws in defect density, defect shape and the ratio of bend to splay energy with respect to the filament stiffness. Finally, they also found that as the rigidity increases, the splay energy stays roughly constant, while the bend energy decreases until the persistence exceeds the filament length and so bend is precluded.

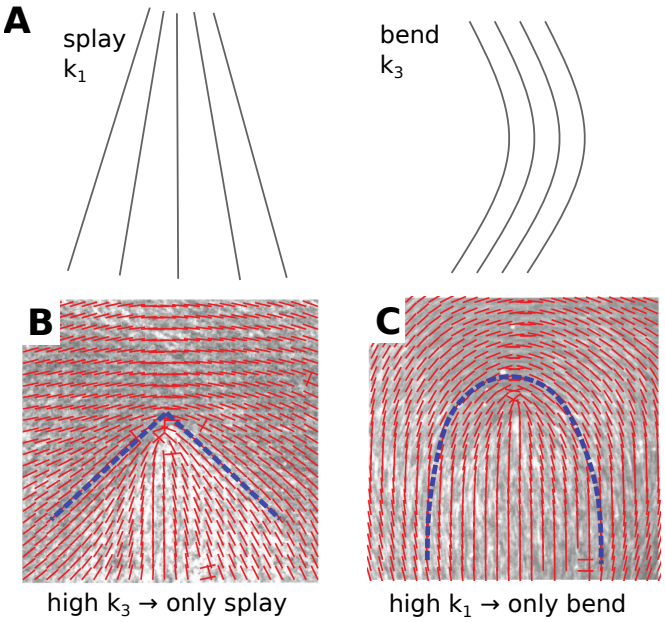

Figure 23: Effect of differing splay and bend constants. **A** illustration of splay and bend deformations and their constants k_1 and k_3, respectively. **B** Defect shape when bend deformations are expensive (k_3 high) – only splay deformations. **C** Defect shape when splay deformations are expensive (k_1 high) – only bend deformations. **B** and **C** from [5].

For this reason we included splay (k_1) and bend (k_3) constants in the calculation of the nematic free energy (as in (8)). As mentioned, this included expressing elastic constants k_1 for splay and k_3 for bend in terms of L_i as done in (9). For ease of understanding, we show the results in terms of the splay constant k_1 and the bend constant k_3.

In this section we explore the effect of varying elasticity. We first investigate the effect of a low or high single elastic constant. Then we look at the influence of differing bend and splay coefficients in various contexts of activity and fluctuations. To this end, we systematically varied the single elastic constant, K, and then the splay and bend constants, k_1 and k_3 for different combinations of $\hat{Q}_{\kappa_B T}$ and ζ. Finally, we

wanted to judge the importance of the 3rd order term in (8).

5.1 Varying single elastic constant

To understand what happens when the elastic constants differ, we first want to see what happens when the single elastic constant is varied. This case corresponds to equal splay and end elastic constants, $k_1 = k_3$. In fact, $L_2 \sim k_1$ (see (9)) and so results that show similar behaviour between varying the single elastic constant, K, or the splay elastic constant, k_1, are not surprising.

5.1.1 Rotational fluctuations

We first investigate the effect of rotational fluctuations (Figure 24). At low elasticity, we see a small but equal dipole, aligned with the defect, in the isotropic stress. The poles of the dipole coincide with the head, the bend region in front of the defect core, and the tail, the splay region behind the defect core. As the elasticity increases, the compressive pole at the head shrinks and disappears as the tensional pole at the tail increases in size and strength. The same dipole disappearance happens when the flow alignment is negative, as the effect of the fluctuations is not inherently extensile or contractile but depends on the flow alignment. The flow pattern retains its shape but grows in size.

5.1.2 Activity

For negative activity, increasing the single elastic constant, K, increases the size and intensity of the isotropic stress and flow patterns (Figure 25), but especially the negative pole at the tail. Note that for positive activity, we see a similar behaviour as for rotational fluctuations, that is disappearance of the dipole to a tensile monopole.

However, when the flow alignment is negative, the picture is reversed and so is the dipole disappearance: positive activity keeps the dipole but strengthens its negative pole, whereas negative activity leads to a tensile monopole. This can be explained by the differing instability of positive and negative activity. While a positive activity leads to instability in bend (at the head), a negative activity leads to an instability in splay (at the tail). This means that a positive activity defect will have the stress exerted at the bend head and the negative activity defect at the splay tail. Then the monopole emerges if the flow alignment is favourable.

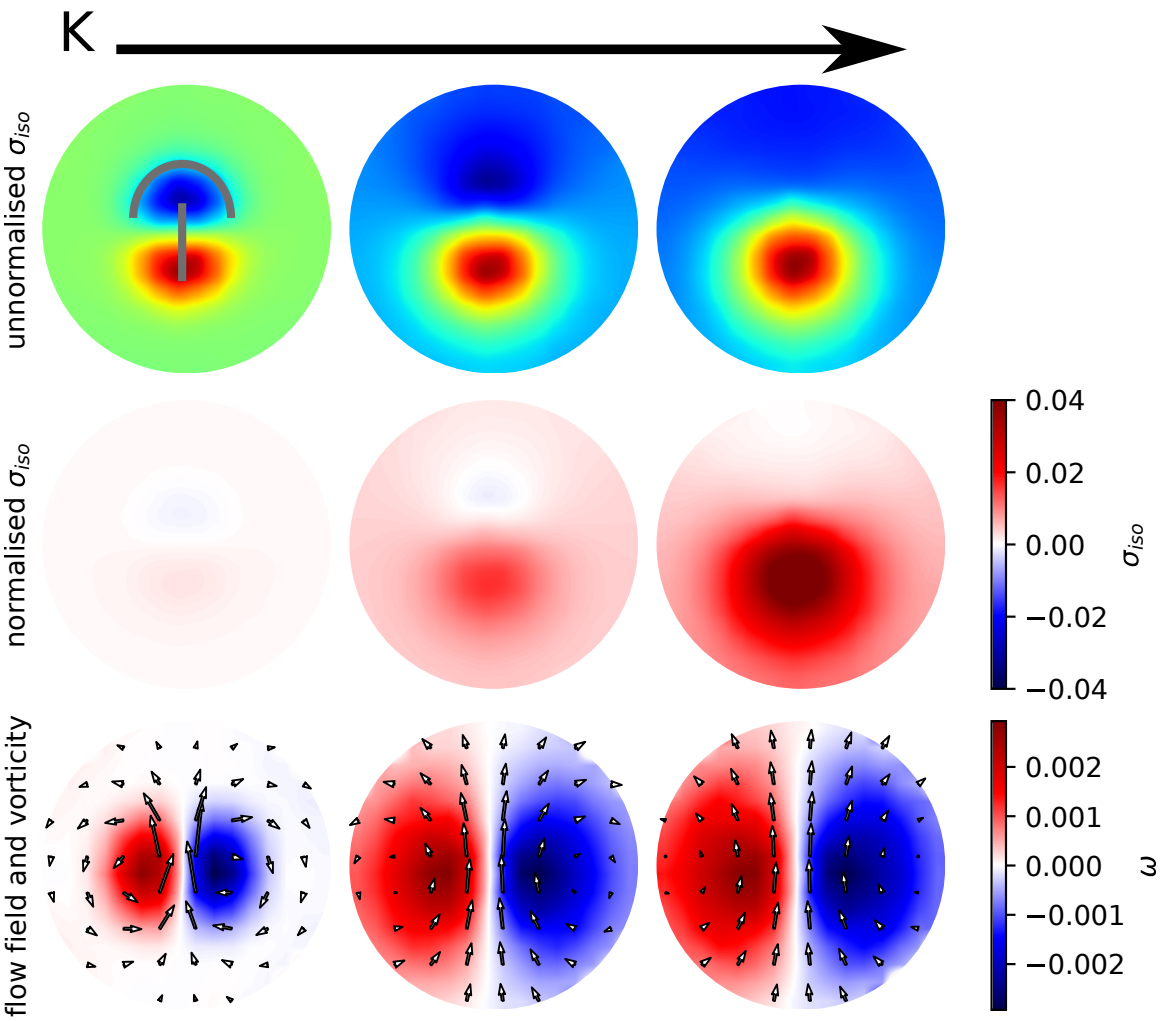

Figure 24: Dipole disappears as the elasticity increases. Low to high elasticity for a system with rotational fluctuation strengths $\hat{Q}_{\kappa_B T} = \{2, 0.67, 0.4\}$ from left to right at $\xi = 1$. Top is the isotropic stress, bottom is the flow field with the vorticity in colour. The contour line denotes the line of $\sigma_{iso} = 0$. Total isotropic stress for columns $1, 2, 3$: $\sigma_{iso,1} = 0.14, \sigma_{iso,2} = 1.0, \sigma_{iso,3} = 2.5$

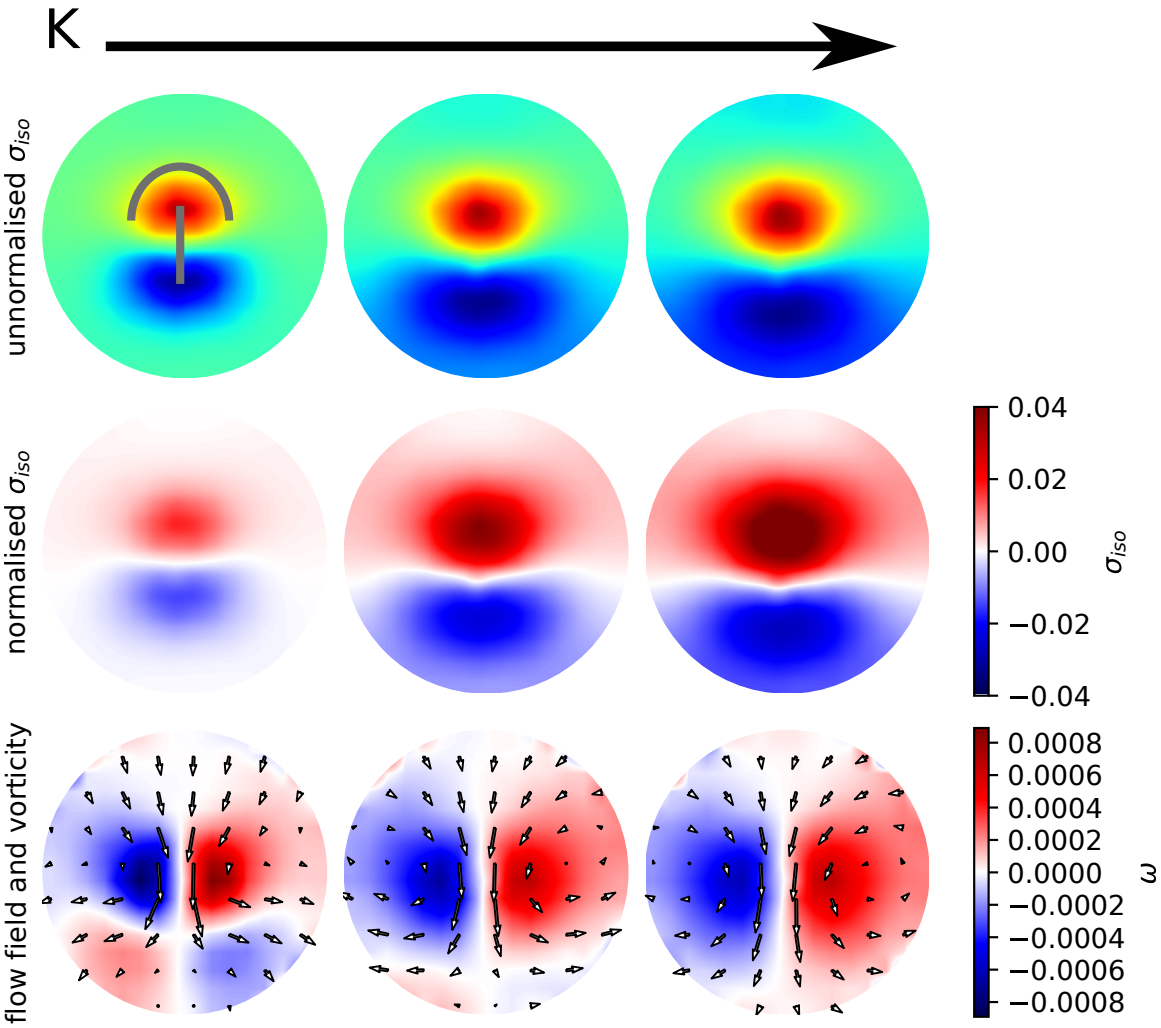

Figure 25: Dipole strength and size increases with elastic constant K. Low to high elasticity for a system with rotational fluctuations $\zeta = -0.05$ at $\xi = 1$. Top is the isotropic stress, bottom is the flow field with the vorticity in colour. The contour line denotes the line of $\sigma_{iso} = 0$. Total isotropic stress for columns $1, 2, 3$: $\sigma_{iso,1} = 0.06, \sigma_{iso,2} = 0.21, \sigma_{iso,3} = 0.55$

5.1.3 Antagonistic fluctuations and activity

However, for negative activity and rotational fluctuations, we see a different behaviour (Figure 26). At low elasticity, K, we see the contractile effect of activity. However as the elasticity increases, the isotropic stress dipole and the flow pattern flip and the defect becomes extensile. We also see the disappearance of the dipole towards a monopole. The behaviour is mirrored for negative flow alignment and positive activity.

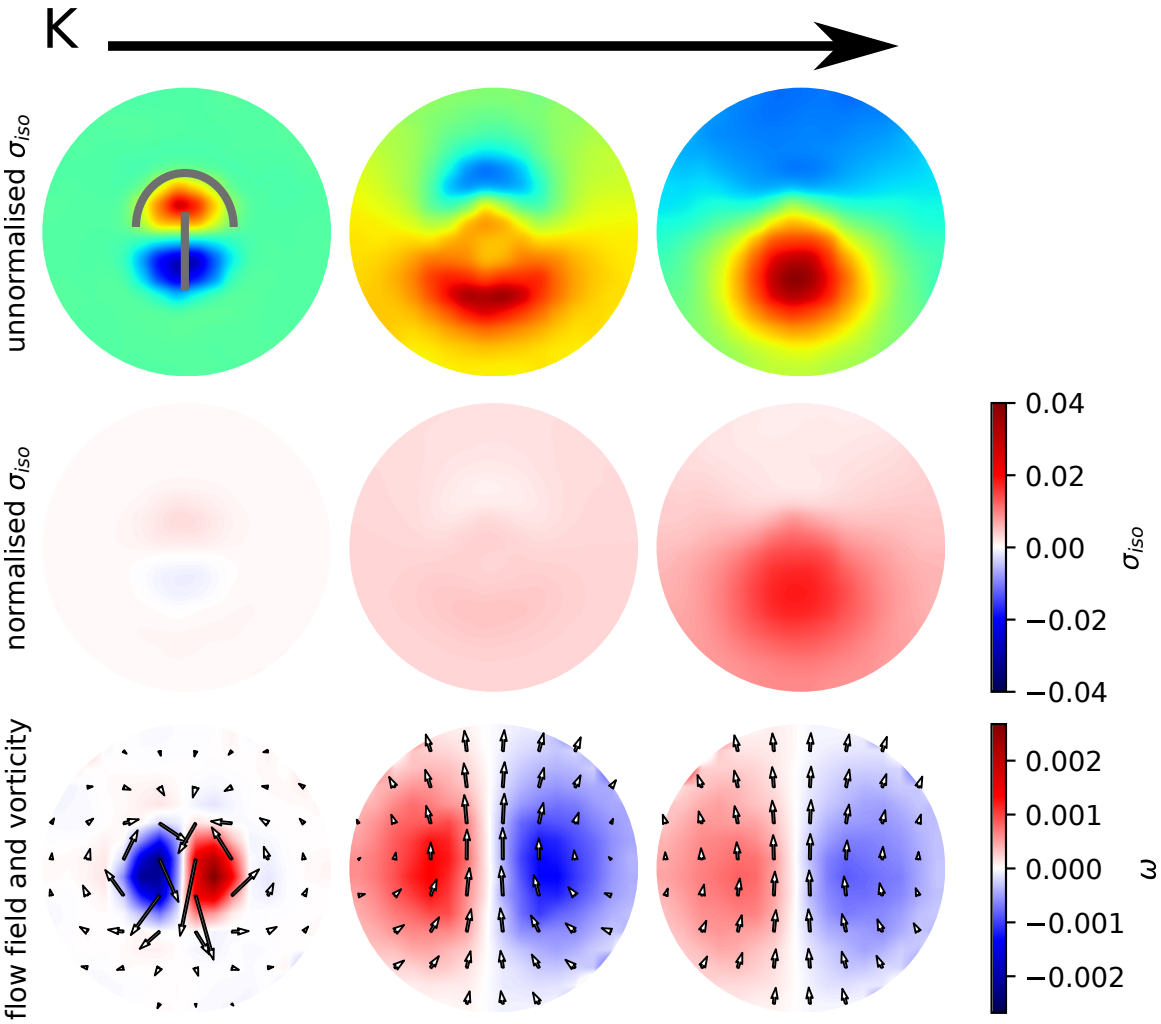

Figure 26: Dipole flips as elasticity increases. The contour line denotes the line of $\sigma_{iso} = 0$. Variation of single elastic constant K for $\hat{Q}_{\kappa_B T} = \{2, 0.67, 0.4\}$ from left to right, and $\zeta = -0.05$. Total isotropic stress for columns $1, 2, 3$: $\sigma_{iso,1} = 0.14, \sigma_{iso,2} = 0.72, \sigma_{iso,3} = 1.6$

What we are seeing, is that at low elasticity, activity dominates. However, with increasing elastic constants, the fluctuation driven effect overwhelms the active effect. When activity and fluctuations are effectively equal but opposite, we can see that the nucleation of defects is suppressed.

5.2 Bend vs Splay

We further wanted to investigate the effect of varying the bend and splay elastic constants, k_3 and k_1 respectively. This is because there is no reason to assume $k_1 = k_3$, as the typical nematogen is an extended object with a clear nematic axis, e.g. rod shaped bacterium or long molecule. This shape immediately suggests different constants, e.g. consider a stiff rod shaped bacterium with little adhesion. The steric interactions prevent bend but not splay. In fact, one study deduced, from the orientation of unbinding defects, that $k_1 < k_3$ in melanocytes [105].

In this section then, we explore the effect of varying bend and splay constants on topological defects. We remind the reader of the elastic free energy with three terms and substitute in the mapping from k_i to L_i to make the relationships explicit:

$$f_{el} = \frac{L_1}{2}\partial_k Q_{ik}\partial_l Q_{il} + \frac{L_2}{2}\partial_k Q_{ij}\partial_k Q_{ij} + \frac{L_3}{2}Q_{ij}\partial_i Q_{kl}\partial_j Q_{kl} \tag{40}$$

$$f_{el} = \frac{-k_1 + k_3}{8S^2}\partial_k Q_{ik}\partial_l Q_{il} + \frac{k_1}{4S^2}\partial_k Q_{ij}\partial_k Q_{ij} + \frac{-k_1 + k_3}{4S^2}Q_{ij}\partial_i Q_{kl}\partial_j Q_{kl}. \tag{41}$$

Note that when $k_3 \neq k_1$, two terms that were 0 now come into play: terms for L_1 and L_3. The L_3 term is of higher order and its relevance is explored in a later section. The L_1 term however, is of the same order and so we don't have an *a priori* idea of its importance.

We find that k_1 generally determines behaviour, e.g. the dipole flip. k_3 has a much smaller role, countering the dipole to monopole transition.

5.2.1 Dipole to Monopole

With only rotational fluctuations ($Q_{\kappa_B T} = 0.04$, resulting in different effective temperatures, detailed in the legend), we increase the splay constant and find that the dipole disappears (Figure 27). Starting with low splay and bend constants ($k_1 = 0.01, k_3 = 0.01$), we see a clear dipole, although the magnitude of the isotropic stress is not large. As splay becomes more dominant, the negative pole at the head disappears and the positive pole at the tail only becomes stronger. This is explained when considering that the head of the defect has mostly bend deformations, and the tail mostly splay. Therefore, when the splay constant dominates over bend, the stresses will develop at the splay region, the tail. The flow field however keeps its qualitative shape, only increasing the size of the double vortex pattern

The same happens for positive activity, which exhibits a dipole with the same polarity which disappears with increasing splay dominance (unpictured). However, for negative activity or rotational fluctuations with negative flow alignment, the dipole does not decrease at all. On the contrary, the negative pole at the tail only gets

stronger. This follows the same explanation that higher stresses will emerge where the elastic constants are higher.

In fact, the behaviour is very similar to that of varying K as in the previous section. This points towards high splay favouring contractile type isotropic stress dipoles, which is shown in the next part.

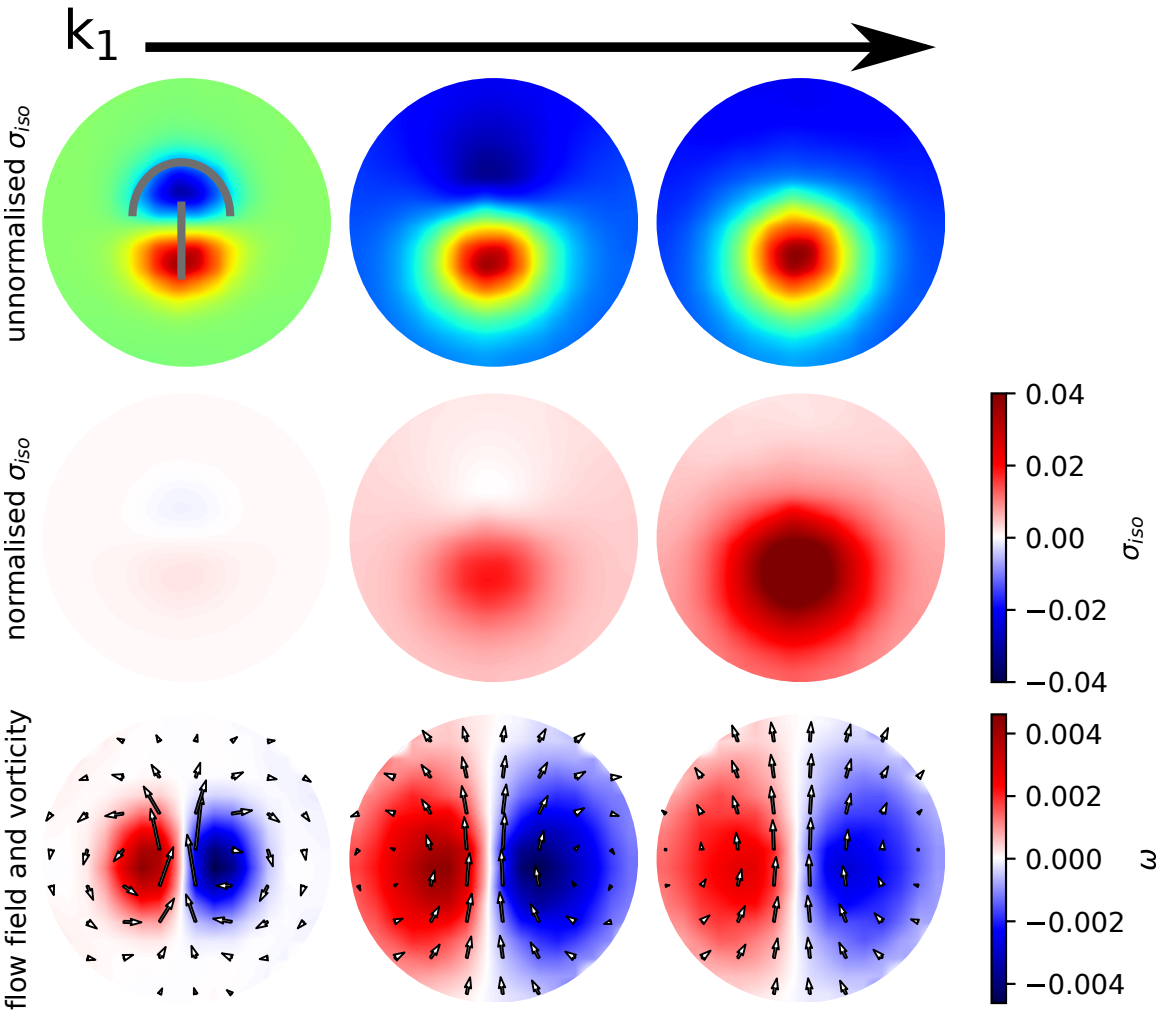

Figure 27: The stress dipole disappears as splay becomes more dominant. The contour line denotes the line of $\sigma_{iso} = 0$. $\hat{Q}_{\kappa_B T} = \{2, 1, 0.67\}, \xi = 1, k_1 \in \{0.01, 0.03, 0.05\}, k_3 = 0.01$ Total isotropic stress for columns $1, 2, 3$: $\sigma_{iso,1} = 0.05, \sigma_{iso,2} = 0.9, \sigma_{iso,3} = 2.5$

The effect of the bend constant, k_3, is opposite but less obvious, because it can be overwhelmed by changes in the splay constant, k_1. So at low splay constant, we vary the bend constant k_3 and see that in contrast to increasing the splay constant k_1, now the negative pole at the head grows stronger (Figure 28). This makes sense because the head is the bend region, so that pole should get stronger as its elastic constant is increased. To quantify this, we summed the total isotropic stress and found that it

decreases with increasing bend constant, k_3.

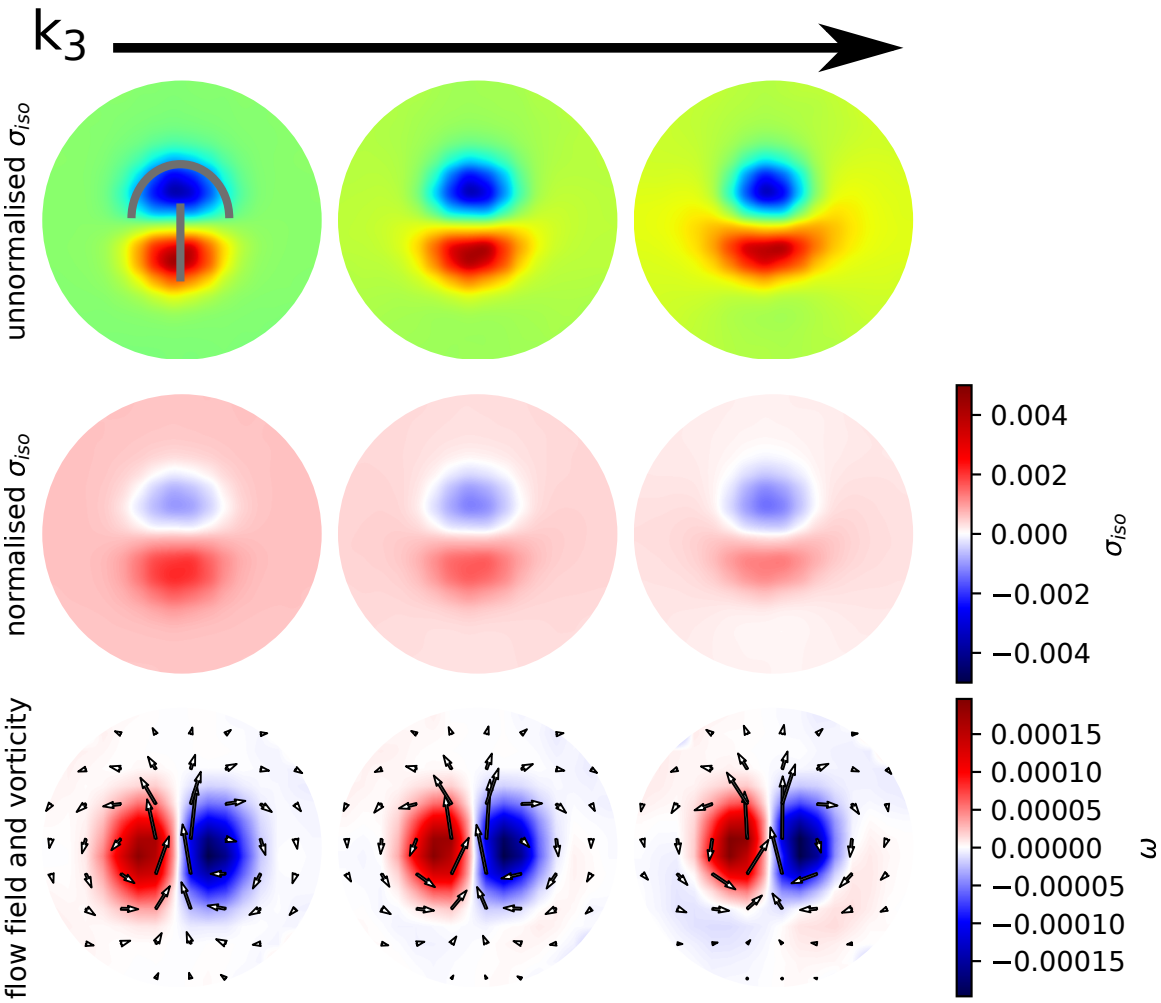

Figure 28: As k_3 increases, the negative pole at the head gets stronger. The contour line denotes the line of $\sigma_{iso} = 0$. $\hat{Q}_{\kappa_B T} = \{2, 1, 0.67\}, \xi = 1, k_1 = 0.01, k_3 \in \{0.01, 0.03, 0.05\}$. Total isotropic stress for columns $1, 2, 3$: $\sigma_{iso,1} = 0.14, \sigma_{iso,2} = 0.09, \sigma_{iso,3} = 0.05$

It is also visible that the defect pattern does not grow in size as with increasing splay constant, k_1, or single elastic constant, K.

5.2.2 Dipole flip with k_1

When we have antagonistic rotational fluctuations and activity, that is the signs of activity and flow alignment are opposite, we can observe a flip in the polarity of the isotropic stress dipole when varying splay vs bend, by keeping bend constant and increasing splay (Figure 29). Note that the isotropic stress magnitude increases.

At low splay, we see a contractile type isotropic stress and flow pattern. This is in line with negative activity. At high splay, we find a isotropic stress pattern very similar to that at 0 activity (rightmost in Figure 27). This is in line with rotational fluctuations at positive flow alignment.

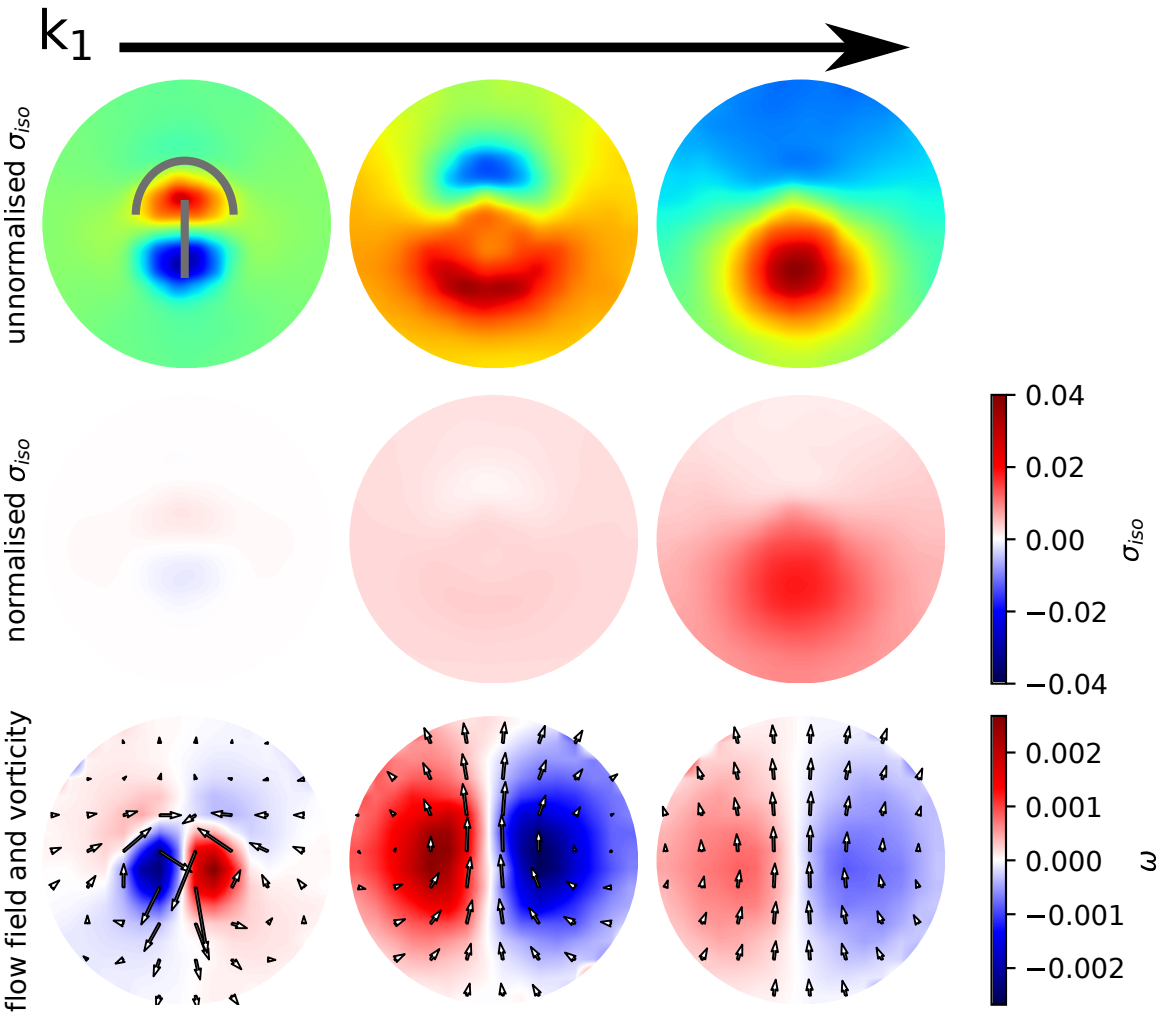

Figure 29: "Dipole" polarity flips as k_1 increases. The contour line denotes the line of $\sigma_{iso} = 0$. $\hat{Q}_{\kappa_B T} = \{0.67, 0.5, 0.4\}, \xi = 1, \zeta = -0.05, k_1 \in \{0.01, 0.03, 0.05\}, k_3 = 0.05$. Total isotropic stress for columns $1, 2, 3$: $\sigma_{iso,1} = 0.05, \sigma_{iso,2} = 0.6, \sigma_{iso,3} = 1.6$

As with varying only K, we see the effect of the activity at low elasticity and of the fluctuations at high elasticity. It is not possible to see the dipole flipping with k_3.

5.3 Importance of L_3

As we developed the elastic free energy in terms of L (8), we expanded in $\mathbf{Q}$ and used two second order terms and one third order term. However, in 2 dimensions, we only

have bend and splay, so only two terms are needed in the k description. Because of the map from k to L, we end up with three terms in the L description. However it is likely that the third order term is less important and we test that here by comparing simulations with and without the third order term. The term is only relevant when $k_1 \neq k_3$, so we look at defects when splay and bend constants are very different.

For only fluctuations or activity there is almost no difference between 2 terms or 3 terms, so we show defect isotropic stress patterns for antagonistic fluctuations and activity (Figure 30).

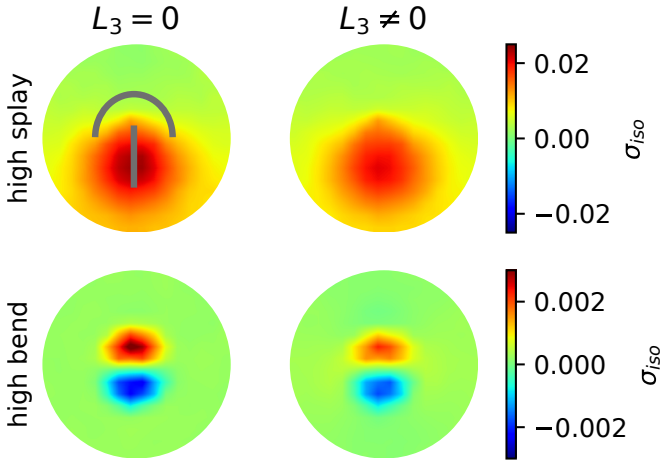

Figure 30: Comparison of simulations without (left) and with (right) L_3 term with antagonistic fluctuations and activity ($\hat{Q}_{\kappa_B T} = 0.67, \xi = 1, \zeta = -0.05$). At high splay (top row, $k_1 = 0.05, k_3 = 0.01$), the patterns are very similar except that when $L_3 = 0$, the stress is slightly higher. The same can be said for high bend (bottom row, $k_1 = 0.01, k_3 = 0.05$), the patterns are very similar, except that the absolute values are slightly higher.

Whether or not we include the L_3 term, does not make a qualitative difference. We have provided some images to show the similarity, but a thorough analysis of the extra term would need a quantitative analysis. It is sufficient to note, that the defect pattern is largely unaffected and so we need not worry about the L_3 term.

5.4 Summary

In this section, we investigated the effect of varying the single elastic constant K, as well as the impact of relaxing the single elastic constant approximation, on the stress patterns around topological defects.

Generally, we saw that varying K or k_1 are very similar, whereas k_3 makes little difference. Regarding the isotropic stress dipole, we saw that increasing K leads to a

loss of the defect for fluctuations or activity, except in the case where flow alignment and activity have opposite signs. When fluctuations and activity were acting against each other, i.e. when fluctuations and activity were added, and flow alignment and activity had opposite signs, we saw the reversal of the dipole with the elasticity. At low elasticity, the activity dominated and we saw the isotropic stress dipole orientation as expected from the activity, whereas at higher elasticity, the fluctuation dominated and we saw the isotropic stress dipole orientation as expected from the fluctuations. Seeing the fluctuations and activity acting at different scales is a valuable insight to the interplay between activity, flow alignment and elasticity. A recent experiment saw that reducing inter-cellular adhesion led to a switch from extensile to contractile behaviour [19]. In this section we have seen how, in reducing elastic effects, the system can switch between contractile and extensile.

6 Discussion and Outlook

In this section, we review the discovery and analysis of motile topological defects in passive nematics and the influence that fluctuation strength, flow alignment and elastic effects have on the defects. We then contextualise the simulations, comparing our observations to those in the literature. Finally, we propose future directions for the work.

Using continuum simulations of a wet, passive nematic, we implemented fluctuations in the hydrodynamical and the nematic field. We found self propelled topological defects for both types of fluctuations. Looking closer at the defects, we saw that the flow field [10, 82, 83] and isotropic stress [10, 19] closely matched those seen in experiment and both continuum [10] and cell based [97] active nematics simulations. We saw that backflow is necessary to the generation of motile defects and that the sign of the flow alignment parameter determines whether the defect movement is extensile or contractile.

The phenomenon of the fluctuation-induced defect chaos phase may be understood as follows: $\pm 1/2$ defect pairs are continually nucleated by fluctuations. The $+1/2$ defect, through elastic interactions, generates a flow field with a jet in the centre, leading to self propulsion. The $+1/2$ defect then propels itself through the fluid, stirring up the director field, thereby favouring further defect creation, until it annihilates with a diffusively moving $-1/2$ defect. This steady state of birth and death of defect pairs is the defect chaos phase.

Having found that the extensile or contractile behaviour of the defects is dependent on the flow alignment, we saw that fluctuations and activity can dominate each other, depending on magnitudes. We showed that, depending on the parameter values, varying only fluctuation strength or activity can lead to a switch from extensile to contractile behaviour, or vice versa. Activity was shown to play a larger role in systems with a low elastic constant, whereas when the single elastic constant was increased, the expected pattern for the fluctuations dominated. Varying the individual bend and splay elastic constants, we demonstrated that an increased value results in increased stress in the bend dominated head or the splay dominated tail, respectively.

6.1 Discussion

Our main contribution is the discovery of the fluctuation-induced defect chaos phase in continuum simulations. Nonetheless, extensile or contractile nematics have been predicted for passive nematics with fluctuations. Killeen, Bertrand and Lee [28] published a paper analytically showing the existence of extensile nematics in passive nematics with fluctuations in the velocity. To test extensility of the system, they looked at $\langle v \cdot (\nabla \cdot \mathbf{Q}) \rangle$, which measures the agreement between the flow and the

direction of nematic splay (the tail region of the defect), so the higher the absolute value, the higher the absolute value of the extensility. The result of their linear stability analysis showed, for flow alignment λ, fluctuation strength Δ and some term $A > 0$:

$$\langle v \cdot (\nabla \cdot \mathbf{Q}) \rangle = -2\lambda\Delta A. \tag{42}$$

So if $\lambda > 0$, the system is extensile, implying that the defects will also be extensile and vice versa, if $\lambda < 0$, the system is contractile, implying that the defects will also be contractile. Our results show that for fluctuations in both velocity or director, active nematics style defect chaos can result. Ours is a more general result, but agrees with [28] that fluctuations in velocity, with a positive flow alignment will lead to extensile active nematics.

We also showed that the backflow effects, the coupling between nematic and hydrodynamic fields, are essential in the extensile or contractile behaviour of the defects. The self-propulsion of $+1/2$ defects in passive nematics with hydrodynamics was seen in [83], where the authors saw that adding hydrodynamics increased the speed of the $+1/2$ defect relative to the speed of the $-1/2$ defect. A recent analytical study [86] suggests that in wet nematics, a $+1/2$ defect will generically generate self propulsion. These studies agree well with our results and our interpretation, that defects are nucleated by fluctuations and propelled by elastic effects interacting with the fluid.

In this way, our results are well supported by recent theoretical studies. However, this work was the first to show the interaction between fluctuations and elasticity to create the defect chaos phase. It is also important to note that this work is based on continuum models. These models are very general, and the equations for the evolution of the nematic and the fluid are widely applicable, not only for cellular systems but 2D wet nematics, such as bacterial collectives [42, 106], microtubule-kinesin motor mixtures [4], actin-myosin complexes [5] and even environmental active fluids such as dense suspensions of phytoplankton or krills [107].

The fluctuating forces that cells exert on their surroundings have been extensively documented [53, 56, 98] and are associated to various sources including, but not limited to, traction force fluctuations exerted by focal adhesions [54, 55, 99], association/dissociation of stress fibers [100], and oscillations in Rho proteins [101, 102]. Fluctuations in orientational order are less well investigated, but the data shows large fluctuations, e.g. in the nematic phase in *Drosophila* pupal wings [93] or measurement of rotational fluctuations in rat embryo fibroblasts [58]. We extensively compared the fluctuations in our model to those observed in biological tissues (Section 4.5) and found that the fluctuation strengths used in the model were of a similar or lower magnitude. Furthermore, the timescales of fluctuation and activity and defect flow fields were found to be on the same order of magnitude as experimental measurements. Finally, we also showed that the fluctuation-induced defects were very similar to those induced by activity in the same continuum model. These comparisons speak to the importance of the fluctuation-induced defects. The discovery, only now, of the

fluctuation-induced defect chaos phase in continuum modelling may be ascribed to the little research into fluctuating wet nematics.

But the extensile or contractile defect chaos is not just a peculiar model effect but has been observed across various biological tissues, including epithelial cells [10, 19, 44], mesothelial cells [29] and fibroblasts [11]. These cells have been characterised as active nematics due to their exhibiting motile $+1/2$ defects, which we have now shown is not uniquely a feature of active nematics. Notably, fibroblasts have been characterised as having low activity [11] and estimation of their effective temperature lined up well with our own effective temperatures. These fibroblasts could then be a system in which fluctuations play a real role in defect dynamics.

In the wet passive nematic, we saw the unbinding of motile $+1/2$ defects, at fluctuation strengths below those required for dry, BKT defect unbinding (Figures 19, 18). Therefore this transition to defect chaos is not the BKT transition. We see then, that bound defect pairs, nucleated by fluctuations, are unbound by elastic effects and that in this case, the $+1/2$ defect is self-propelled. This transition deserves investigation.

When we consider that fluctuations are ubiquitous, both generically as a feature of non-idealised systems and measured across biology [47, 53, 56, 57], it is right to investigate active nematics in the presence of fluctuations. In doing this, we saw that, at large ranges of activity and fluctuation strengths, the effect of one or the other dominates the appearance of the defect chaos (Figure 21). For example, large fluctuations creating an extensile defect chaos phase even when the activity was negative. However, if we imagine that a cell or tissue operates near the boundary between the extensile and contractile phases, the cell can easily switch between contractile and extensile behaviour. Activity, as an active process of the cell, is available for the cell to change and has been observed to vary as the tissue develops [103]. Similarly, fluctuation strength can be controlled by the cells themselves, as the fluctuations are not thermal but actually also active process of the cell such as fluctuating focal adhesion protrusion [53, 55]. We also saw that when activity and fluctuations were acting in opposite directions, i.e. when the signs of activity and flow alignment were not the same, the generation of defects could be entirely suppressed. This adds an extra dimension to the agency of the tissue – complete suppression of defect chaos at the right activity and fluctuation strength, with easy access to the contractile or extensile phase.

Elasticity of the nematic is another parameter that can be varied across different cell types or varied by cells themselves [105, 108]. We found that, when increasing the single elastic constant for a fluctuating system, an isotropic stress dipole would turn into a monopole, with only tension at the tail. For an active system however, depending on the flow alignment, the dipole could either disappear or grow stronger. In light of the functional role that the stress around the defect plays, such as effecting cell extrusion [10], control of the defect isotropic stress pattern by changing the elasti-

city is an interesting observation. We found that when both fluctuations and activity were present, at low elasticity, the activity dominated the defect flow and isotropic stress patterns, but with increasing elasticity, the fluctuation-induced pattern became stronger, finally dominating. This effect of activity and fluctuations having different impacts at different elasticities is an interesting insight into the interplay between these factors. It also gives another option for a tissue to switch from extensile to contractile, reducing inter-cellular elastic effects by, e.g. reducing inter-cellular adhesion or connection.

We have now seen multiple ways in which the tissue could switch from extensile to contractile, by changing fluctuation strength, activity or the elastic constant. A recent study investigated the active nematic behaviour of an MDCK monolayer [19] and knocked out a key cell-cell adhesion protein. This reduction in inter-cellular adhesion led to a flip of the isotropic stress pattern, just as we have seen. This points towards a change in the elastic constant, as now cells have less adhesion to their neighbours and therefore less force transmission, resulting in smaller elastic effects. However, one might also point out that, by uncoupling the cell from its neighbours, it is free to change its shape more freely and therefore fluctuations could play more of a role.

6.2 Outlook

The main result of this work – the discovery of the defect chaos phase generated by fluctuations and perpetuated by elastic effects – opens up a lot of potential research directions both theoretically and experimentally. In particular, characterisation of the transition from nematic order to defect chaos and characterisation of the fluctuation and elasticity driven defect chaos.

As we have seen, the transition to defect chaos happens at lower fluctuation strength than the BKT transition and it would be very interesting to explore this further and possibly place this transition into a universality class. A further characterisation of the fluctuation driven defect chaos phase, by e.g. correlation or structure functions might reveal differences to the active nematic defect chaos phase. This would suggest a combined experimental and computational study to find out which cell layers are actively driven and which are fluctuation driven.

References

[1] Amin Doostmohammadi and Benoit Ladoux. 'Physics of liquid crystals in cell biology'. In: *Trends in Cell Biology* (Oct. 2021). DOI: 10.1016/j.tcb.2021.09.012.

[2] M. C. Marchetti et al. 'Hydrodynamics of soft active matter'. In: *Reviews of Modern Physics* 85.3 (19th July 2013). Publisher: American Physical Society, pp. 1143–1189. DOI: 10.1103/RevModPhys.85.1143.

[3] Tariq Butt et al. 'Myosin Motors Drive Long Range Alignment of Actin Filaments 2'. In: *Journal of Biological Chemistry* 285.7 (12th Feb. 2010). Publisher: Elsevier, pp. 4964–4974. DOI: 10.1074/jbc.M109.044792.

[4] Tim Sanchez et al. 'Spontaneous motion in hierarchically assembled active matter'. In: *Nature* 491.7424 (Nov. 2012), pp. 431–434. DOI: 10.1038/nature11591.

[5] Rui Zhang et al. 'Interplay of structure, elasticity, and dynamics in actin-based nematic materials'. In: *Proceedings of the National Academy of Sciences* 115.2 (9th Jan. 2018), E124–E133. DOI: 10.1073/pnas.1713832115.

[6] Yonit Maroudas-Sacks et al. 'Topological defects in the nematic order of actin fibres as organization centres of Hydra morphogenesis'. In: *Nature Physics* 17.2 (Feb. 2021), pp. 251–259. DOI: 10.1038/s41567-020-01083-1.

[7] D. Dell'Arciprete et al. 'A growing bacterial colony in two dimensions as an active nematic'. In: *Nature Communications* 9.1 (Dec. 2018), p. 4190. DOI: 10.1038/s41467-018-06370-3.

[8] Zhihong You et al. 'Geometry and Mechanics of Microdomains in Growing Bacterial Colonies'. In: *Physical Review X* 8.3 (12th Sept. 2018), p. 031065. DOI: 10.1103/PhysRevX.8.031065.

[9] Katherine Copenhagen et al. 'Topological defects promote layer formation in Myxococcus xanthus colonies'. In: *Nature Physics* 17.2 (Feb. 2021). Number: 2 Publisher: Nature Publishing Group, pp. 211–215. DOI: 10.1038/s41567-020-01056-4.

[10] Thuan Beng Saw et al. 'Topological defects in epithelia govern cell death and extrusion'. In: *Nature* 544.7649 (13th Apr. 2017), pp. 212–216. DOI: 10.1038/nature21718.

[11] Guillaume Duclos et al. 'Topological defects in confined populations of spindle-shaped cells'. In: *Nature Physics* 13.1 (Jan. 2017), pp. 58–62. DOI: 10.1038/nphys3876.

[12] Kyogo Kawaguchi, Ryoichiro Kageyama and Masaki Sano. 'Topological defects control collective dynamics in neural progenitor cell cultures'. In: *Nature* 545.7654 (May 2017). Number: 7654 Publisher: Nature Publishing Group, pp. 327–331. DOI: 10.1038/nature22321.

[13] Suraj Shankar et al. 'Topological active matter'. In: *arXiv:2010.00364 [cond-mat]* (13th Oct. 2020). arXiv: 2010.00364.

[14] Mark J. Bowick et al. 'Symmetry, Thermodynamics and Topology in Active Matter'. In: *arXiv:2107.00724 [cond-mat]* (7th Aug. 2021). arXiv: 2107.00724.

[15] Sriram Ramaswamy. 'The Mechanics and Statistics of Active Matter'. In: *Annual Review of Condensed Matter Physics* 1.1 (10th Aug. 2010), pp. 323–345. DOI: 10.1146/annurev-conmatphys-070909-104101.

[16] Shradha Mishra, R. Aditi Simha and Sriram Ramaswamy. 'A dynamic renormalization group study of active nematics'. In: *Journal of Statistical Mechanics: Theory and Experiment* 2010.2 (Feb. 2010). Publisher: IOP Publishing, P02003. DOI: 10.1088/1742-5468/2010/02/P02003.

[17] Suraj Shankar, Sriram Ramaswamy and M. Cristina Marchetti. 'Low-noise phase of a two-dimensional active nematic system'. In: *Physical Review E* 97.1 (29th Jan. 2018). Publisher: American Physical Society, p. 012707. DOI: 10.1103/PhysRevE.97.012707.

[18] Amin Doostmohammadi et al. 'Active nematics'. In: *Nature Communications* 9.1 (Dec. 2018), p. 3246. DOI: 10.1038/s41467-018-05666-8.

[19] Lakshmi Balasubramaniam et al. 'Investigating the nature of active forces in tissues reveals how contractile cells can form extensile monolayers'. In: *Nature Materials* (18th Feb. 2021). Publisher: Nature Publishing Group, pp. 1–11. DOI: 10.1038/s41563-021-00919-2.

[20] P. M. Chaikin and T. C. Lubensky. *Principles of Condensed Matter Physics*. 1st ed. Cambridge University Press, 22nd June 1995. ISBN: 978-0-511-81346-7. DOI: 10.1017/CBO9780511813467.

[21] D. L. Stein. 'Kosterlitz-Thouless phase transitions in two-dimensional liquid crystals'. In: *Physical Review B* 18.5 (1st Sept. 1978), pp. 2397–2399. DOI: 10.1103/PhysRevB.18.2397.

[22] R. L.C. Vink. 'The isotropic-to-nematic transition in a two-dimensional fluid of hard needles: a finite-size scaling study'. In: *The European Physical Journal B* 72.2 (Nov. 2009), pp. 225–231. DOI: 10.1140/epjb/e2009-00333-x.

[23] D. Frenkel and R. Eppenga. 'Evidence for algebraic orientational order in a two-dimensional hard-core nematic'. In: *Physical Review A* 31.3 (1st Mar. 1985), pp. 1776–1787. DOI: 10.1103/PhysRevA.31.1776.

[24] Martin A. Bates and Daan Frenkel. 'Phase behavior of two-dimensional hard rod fluids'. In: *The Journal of Chemical Physics* 112.22 (8th June 2000), pp. 10034–10041. DOI: 10.1063/1.481637.

[25] Hugues Chaté, Francesco Ginelli and Raúl Montagne. 'Simple Model for Active Nematics: Quasi-Long-Range Order and Giant Fluctuations'. In: *Physical Review Letters* 96.18 (9th May 2006), p. 180602. DOI: 10.1103/PhysRevLett.96.180602.

[26] Suraj Shankar et al. 'Defect Unbinding in Active Nematics'. In: *Physical Review Letters* 121.10 (7th Sept. 2018), p. 108002. DOI: 10.1103/PhysRevLett.121.108002.

[27] Farzan Vafa et al. 'Fluctuations can induce local nematic order and extensile stress in monolayers of motile cells'. In: *Soft Matter* 17.11 (25th Mar. 2021). Publisher: The Royal Society of Chemistry, pp. 3068–3073. DOI: 10.1039/D0SM02027C.

[28] Andrew Killeen, Thibault Bertrand and Chiu Fan Lee. 'Polar Fluctuations Lead to Extensile Nematic Behavior in Confluent Tissues'. In: *Physical Review Letters* 128.7 (15th Feb. 2022), p. 078001. DOI: 10.1103/PhysRevLett.128.078001.

[29] Guanming Zhang and Julia M. Yeomans. 'Active forces in confluent cell monolayers'. In: *arXiv:2111.14401 [cond-mat, physics:physics]* (29th Nov. 2021). arXiv: 2111.14401.

[30] J. Prost, F. Jülicher and J-F. Joanny. 'Active gel physics'. In: *Nature Physics* 11.2 (Feb. 2015), pp. 111–117. DOI: 10.1038/nphys3224.

[31] Étienne Fodor and M. Cristina Marchetti. 'The statistical physics of active matter: From self-catalytic colloids to living cells'. In: *Physica A: Statistical Mechanics and its Applications* 504 (Aug. 2018), pp. 106–120. DOI: 10.1016/j.physa.2017.12.137.

[32] V. Narayan, S. Ramaswamy and N. Menon. 'Long-Lived Giant Number Fluctuations in a Swarming Granular Nematic'. In: *Science* 317.5834 (6th July 2007), pp. 105–108. DOI: 10.1126/science.1140414.

[33] Michael E. Cates and Julien Tailleur. 'Motility-Induced Phase Separation'. In: *Annual Review of Condensed Matter Physics* 6.1 (1st Mar. 2015), pp. 219–244. DOI: 10.1146/annurev-conmatphys-031214-014710.

[34] S.P. Thampi and J.M. Yeomans. 'Active turbulence in active nematics'. In: *The European Physical Journal Special Topics* 225.4 (July 2016), pp. 651–662. DOI: 10.1140/epjst/e2015-50324-3.

[35] Stephen J. DeCamp et al. 'Orientational order of motile defects in active nematics'. In: *Nature Materials* 14.11 (Nov. 2015), pp. 1110–1115. DOI: 10.1038/nmat4387.

[36] Henricus H. Wensink et al. 'Meso-scale turbulence in living fluids'. In: *Proceedings of the National Academy of Sciences* 109.36 (4th Sept. 2012), pp. 14308–14313. DOI: 10.1073/pnas.1202032109.

[37] Hugues Chaté. 'Dry Aligning Dilute Active Matter'. In: *Annual Review of Condensed Matter Physics* 11.1 (10th Mar. 2020), pp. 189–212. DOI: 10.1146/annurev-conmatphys-031119-050752.

[38] M. Reza Shaebani et al. 'Computational models for active matter'. In: *Nature Reviews Physics* 2.4 (Apr. 2020), pp. 181–199. DOI: 10.1038/s42254-020-0152-1. arXiv: 1910.02528.

[39] Thuan Beng Saw et al. 'Biological Tissues as Active Nematic Liquid Crystals'. In: *Advanced Materials* 30.47 (2018), p. 1802579. DOI: 10.1002/adma.201802579.

[40] Lakshmi Balasubramaniam, René-Marc Mège and Benoît Ladoux. 'Active nematics across scales from cytoskeleton organization to tissue morphogenesis'. In: *Current Opinion in Genetics & Development* 73 (Apr. 2022), p. 101897. DOI: 10.1016/j.gde.2021.101897.

[41] G. Duclos et al. 'Perfect nematic order in confined monolayers of spindle-shaped cells'. In: *Soft Matter* 10.14 (2014), pp. 2346–2353. DOI: 10.1039/C3SM52323C.

[42] O. J. Meacock et al. 'Bacteria solve the problem of crowding by moving slowly'. In: *Nature Physics* 17.2 (Feb. 2021), pp. 205–210. DOI: 10.1038/s41567-020-01070-6.

[43] R. Aditi Simha and Sriram Ramaswamy. 'Hydrodynamic Fluctuations and Instabilities in Ordered Suspensions of Self-Propelled Particles'. In: *Physical Review Letters* 89.5 (15th July 2002), p. 058101. DOI: 10.1103/PhysRevLett.89.058101.

[44] C. Blanch-Mercader et al. 'Turbulent Dynamics of Epithelial Cell Cultures'. In: *Physical Review Letters* 120.20 (17th May 2018), p. 208101. DOI: 10.1103/PhysRevLett.120.208101.

[45] Jun Zhang et al. 'Topological defects in the mesothelium suppress ovarian cancer cell clearance'. In: *APL Bioengineering* 5.3 (1st Sept. 2021), p. 036103. DOI: 10.1063/5.0047523.

[46] Surabhi Sonam et al. 'Mechanical stress driven by rigidity sensing governs epithelial stability'. In: (12th Mar. 2022). DOI: 10.1101/2022.03.10.483785.

[47] Lev S Tsimring. 'Noise in biology'. In: *Reports on Progress in Physics* 77.2 (1st Feb. 2014), p. 026601. DOI: 10.1088/0034-4885/77/2/026601.

[48] Avigdor Eldar and Michael B. Elowitz. 'Functional roles for noise in genetic circuits'. In: *Nature* 467.7312 (Sept. 2010), pp. 167–173. DOI: 10.1038/nature09326.

[49] Denise Serra et al. 'Self-organization and symmetry breaking in intestinal organoid development'. In: *Nature* 569.7754 (May 2019), pp. 66–72. DOI: 10.1038/s41586-019-1146-y.

[50] Alan Hastings et al. 'Transient phenomena in ecology'. In: *Science* 361.6406 (7th Sept. 2018). DOI: 10.1126/science.aat6412.

[51] Jan A. Freund et al. 'Bloom dynamics in a seasonally forced phytoplankton–zooplankton model: Trigger mechanisms and timing effects'. In: *Ecological Complexity* 3.2 (June 2006), pp. 129–139. DOI: 10.1016/j.ecocom.2005.11.001.

[52] Matej Krajnc. 'Solid–fluid transition and cell sorting in epithelia with junctional tension fluctuations'. In: *Soft Matter* 16.13 (2020). Publisher: Royal Society of Chemistry, pp. 3209–3215. DOI: 10.1039/C9SM02310K.

[53] Sergey V Plotnikov and Clare M Waterman. 'Guiding cell migration by tugging'. In: *Current Opinion in Cell Biology* 25.5 (Oct. 2013), pp. 619–626. DOI: 10.1016/j.ceb.2013.06.003.

[54] Zeno Messi et al. 'Traction Forces Control Cell-Edge Dynamics and Mediate Distance Sensitivity during Cell Polarization'. In: *Current Biology* 30.9 (May 2020), 1762–1769.e5. DOI: 10.1016/j.cub.2020.02.078.

[55] Sergey V. Plotnikov et al. 'Force Fluctuations within Focal Adhesions Mediate ECM-Rigidity Sensing to Guide Directed Cell Migration'. In: *Cell* 151.7 (Dec. 2012), pp. 1513–1527. DOI: 10.1016/j.cell.2012.11.034.

[56] Scott Curran et al. 'Myosin II Controls Junction Fluctuations to Guide Epithelial Tissue Ordering'. In: *Developmental Cell* 43.4 (Nov. 2017), 480–492.e6. DOI: 10.1016/j.devcel.2017.09.018.

[57] Steven M. Zehnder et al. 'Cell Volume Fluctuations in MDCK Monolayers'. In: *Biophysical Journal* 108.2 (Jan. 2015), pp. 247–250. DOI: 10.1016/j.bpj.2014.11.1856.

[58] Avraham Moriel, Ariel Livne and Eran Bouchbinder. 'Cellular orientational fluctuations, rotational diffusion and nematic order under periodic driving'. In: *bioRxiv* (1st May 2022), p. 13. DOI: 10.1101/2022.04.30.490160.

[59] Eric Bertin et al. 'Mesoscopic theory for fluctuating active nematics'. In: *New Journal of Physics* 15.8 (28th Aug. 2013), p. 085032. DOI: 10.1088/1367-2630/15/8/085032.

[60] Lasse Bonn et al. 'Fluctuation-induced features of topological defects in passive nematics'. In: *arXiv:2201.05338 [cond-mat, physics:physics]* (14th Jan. 2022). arXiv: 2201.05338.

[61] Nigel J. Mottram and Christopher J. P. Newton. 'Introduction to Q-tensor theory'. In: *arXiv:1409.3542 [cond-mat]* (12th Sept. 2014). arXiv: 1409.3542.

[62] Maurice Kléman and Oleg D. Lavrentovich. *Soft matter physics: an introduction*. Partially ordered systems. New York: Springer, 2003. 637 pp. ISBN: 978-0-387-95267-3.

[63] Pierre Gilles de Gennes and Jacques Prost. *The physics of liquid crystals*. 2nd ed. Oxford science publications 83. Oxford : New York: Clarendon Press ; Oxford University Press, 1993. 597 pp. ISBN: 978-0-19-852024-5.

[64] B. J. Edwards and A. N. Beris. 'Note: Order Parameter Representation of Spatial Inhomogeneities of Polymeric Liquid Crystals'. In: *Journal of Rheology* 33.7 (Oct. 1989), pp. 1189–1193. DOI: 10.1122/1.550070.

[65] Antony N. Beris and Brian J. Edwards. *Thermodynamics of flowing systems: with internal microstructure*. Oxford engineering science series 36. New York: Oxford University Press, 1994. 683 pp. ISBN: 978-0-19-507694-3.

[66] K. Schiele and S. Trimper. 'On the Elastic Constants of a Nematic Liquid Crystal'. In: *physica status solidi (b)* 118.1 (1983), pp. 267–274. DOI: 10.1002/pssb.2221180132.

[67] Kristian Thijssen, Mehrana R. Nejad and Julia M. Yeomans. 'Role of Friction in Multidefect Ordering'. In: *Physical Review Letters* 125.21 (20th Nov. 2020). Publisher: American Physical Society, p. 218004. DOI: 10.1103/PhysRevLett.125.218004.

[68] Benoît Aigouy et al. 'Cell Flow Reorients the Axis of Planar Polarity in the Wing Epithelium of Drosophila'. In: *Cell* 142.5 (Sept. 2010), pp. 773–786. DOI: 10.1016/j.cell.2010.07.042.

[69] G. Duclos et al. 'Spontaneous shear flow in confined cellular nematics'. In: *Nature Physics* 14.7 (July 2018), pp. 728–732. DOI: 10.1038/s41567-018-0099-7.

[70] Luca Giomi et al. 'Defect Annihilation and Proliferation in Active Nematics'. In: *Physical Review Letters* 110.22 (29th May 2013), p. 228101. DOI: 10.1103/PhysRevLett.110.228101.

[71] Julia M. Yeomans. 'The Hydrodynamics of Active Systems'. In: *La Rivista del Nuovo Cimento* 40.1 (29th Dec. 2016), pp. 1–31. DOI: 10.1393/ncr/i2016-10131-5. arXiv: 1603.00194.

[72] Knut Drescher et al. 'Direct Measurement of the Flow Field around Swimming Microorganisms'. In: *Physical Review Letters* 105.16 (11th Oct. 2010). Publisher: American Physical Society, p. 168101. DOI: 10.1103/PhysRevLett.105.168101.

[73] Knut Drescher et al. 'Fluid dynamics and noise in bacterial cell–cell and cell–surface scattering'. In: *Proceedings of the National Academy of Sciences* 108.27 (5th July 2011), pp. 10940–10945. DOI: 10.1073/pnas.1019079108.

[74] David Saintillan. 'Rheology of Active Fluids'. In: *Annual Review of Fluid Mechanics* 50.1 (5th Jan. 2018), pp. 563–592. DOI: 10.1146/annurev-fluid-010816-060049.

[75] Ananyo Maitra et al. 'A nonequilibrium force can stabilize 2D active nematics'. In: *Proceedings of the National Academy of Sciences* 115.27 (3rd July 2018), pp. 6934–6939. DOI: 10.1073/pnas.1720607115.

[76] Ricard Alert, Jaume Casademunt and Jean-François Joanny. 'Active Turbulence'. In: *Annual Review of Condensed Matter Physics* 13.1 (2022), null. DOI: 10.1146/annurev-conmatphys-082321-035957.

[77] L. N. Carenza, L. Biferale and G. Gonnella. 'Cascade or not cascade? Energy transfer and elastic effects in active nematics'. In: *Europhysics Letters* 132.4 (Nov. 2020). Publisher: IOP Publishing, p. 44003. DOI: 10.1209/0295-5075/132/44003.

[78] Ricard Alert, Jean-François Joanny and Jaume Casademunt. 'Universal scaling of active nematic turbulence'. In: *Nature Physics* 16.6 (June 2020), pp. 682–688. DOI: 10.1038/s41567-020-0854-4. arXiv: 1906.04757.

[79] Jonas Rønning et al. 'Flow around topological defects in active nematic films'. In: *arXiv:2111.08537 [cond-mat]* (16th Nov. 2021). arXiv: 2111.08537.

[80] Louis Brézin, Thomas Risler and Jean-François Joanny. 'Spontaneous flow created by active topological defects'. In: *arXiv:2202.00646 [cond-mat, physics:physics]* (1st Feb. 2022). arXiv: 2202.00646.

[81] Yi-Heng Zhang, Markus Deserno and Zhan-Chun Tu. 'Dynamics of active nematic defects on the surface of a sphere'. In: *Physical Review E* 102.1 (17th July 2020), p. 012607. DOI: 10.1103/PhysRevE.102.012607.

[82] Luca Giomi et al. 'Defect dynamics in active nematics'. In: *Philosophical Transactions of the Royal Society A: Mathematical, Physical and Engineering Sciences* 372.2029 (28th Nov. 2014), p. 20130365. DOI: 10.1098/rsta.2013.0365.

[83] Géza Tóth, Colin Denniston and J. M. Yeomans. 'Hydrodynamics of Topological Defects in Nematic Liquid Crystals'. In: *Physical Review Letters* 88.10 (26th Feb. 2002), p. 105504. DOI: 10.1103/PhysRevLett.88.105504.

[84] Suraj Shankar and M. Cristina Marchetti. 'Hydrodynamics of Active Defects: From Order to Chaos to Defect Ordering'. In: *Physical Review X* 9.4 (4th Dec. 2019). Publisher: American Physical Society, p. 041047. DOI: 10.1103/PhysRevX.9.041047.

[85] Kristian Thijssen et al. 'Active nematics with anisotropic friction: the decisive role of the flow aligning parameter'. In: *Soft Matter* 16.8 (2020). Publisher: Royal Society of Chemistry, pp. 2065–2074. DOI: 10.1039/C9SM01963D.

[86] Dimitrios Krommydas, Livio Carenza and Luca Giomi. 'Passive self-propulsion and enhanced annihilation of $p-$atic defects'. In: *arXiv:2203.06170 [cond-mat]* (11th Mar. 2022). arXiv: 2203.06170.

[87] D. Marenduzzo et al. 'Steady-state hydrodynamic instabilities of active liquid crystals: Hybrid lattice Boltzmann simulations'. In: *Physical Review E* 76.3 (24th Sept. 2007), p. 031921. DOI: 10.1103/PhysRevE.76.031921.

[88] Amin Doostmohammadi et al. 'Onset of meso-scale turbulence in active nematics'. In: *Nature Communications* 8.1 (Aug. 2017), p. 15326. DOI: 10.1038/ncomms15326.

[89] Guillaume Duclos et al. 'Topological structure and dynamics of three-dimensional active nematics'. In: *Science* 367.6482 (6th Mar. 2020). Publisher: American Association for the Advancement of Science, pp. 1120–1124. DOI: 10.1126/science.aaz4547.

[90] Timm Krüger et al. *The Lattice Boltzmann Method: Principles and Practice*. Graduate Texts in Physics. Cham: Springer International Publishing, 2017. ISBN: 978-3-319-44649-3. DOI: 10.1007/978-3-319-44649-3.

[91] R Adhikari et al. 'Fluctuating lattice Boltzmann'. In: *Europhysics Letters (EPL)* 71.3 (Aug. 2005), pp. 473–479. DOI: 10.1209/epl/i2004-10542-5.

[92] Burkhard Dünweg, Ulf D. Schiller and Anthony J. C. Ladd. 'Statistical mechanics of the fluctuating lattice Boltzmann equation'. In: *Physical Review E* 76.3 (12th Sept. 2007). Publisher: American Physical Society, p. 036704. DOI: 10.1103/PhysRevE.76.036704.

[93] Mark Olenik et al. 'Fluctuations, geometry and non-equilibrium thermodynamics of living epithelial tissue'. In: *arXiv:2201.07154 [cond-mat]* (18th Jan. 2022). arXiv: 2201.07154.

[94] Arthur J. Vromans and Luca Giomi. 'Orientational properties of nematic disclinations'. In: *Soft Matter* 12.30 (27th July 2016). Publisher: The Royal Society of Chemistry, pp. 6490–6495. DOI: 10.1039/C6SM01146B.

[95] Sumesh P. Thampi, Ramin Golestanian and Julia M. Yeomans. 'Instabilities and topological defects in active nematics'. In: *EPL (Europhysics Letters)* 105.1 (Jan. 2014). Publisher: IOP Publishing, p. 18001. DOI: 10.1209/0295-5075/105/18001.

[96] Lasse Bonn. *Motile Defects Supplementary Videos - Dropbox*. URL: https://www.dropbox.com/sh/5e4u33h9ppo00tu/AAC95_5iZQrYZ__-QwJQ33cqa?dl=0 (visited on 19/05/2022).

[97] Romain Mueller, Julia M. Yeomans and Amin Doostmohammadi. 'Emergence of Active Nematic Behavior in Monolayers of Isotropic Cells'. In: *Physical Review Letters* 122.4 (1st Feb. 2019), p. 048004. DOI: 10.1103/PhysRevLett.122.048004.

[98] Yi-An Yang et al. 'Local contractions regulate E-cadherin rigidity sensing'. In: *Science Advances* 8.4 (28th Jan. 2022). DOI: 10.1126/sciadv.abk0387.

[99] Lin Ji, James Lim and Gaudenz Danuser. 'Fluctuations of intracellular forces during cell protrusion'. In: *Nature Cell Biology* 10.12 (Dec. 2008). Number: 12 Publisher: Nature Publishing Group, pp. 1393–1400. DOI: 10.1038/ncb1797.

[100] Louise Guolla et al. 'Force transduction and strain dynamics in actin stress fibres in response to nanonewton forces'. In: *Journal of Cell Science* 125.3 (1st Feb. 2012), pp. 603–613. DOI: 10.1242/jcs.088302.

[101] Matthias Machacek et al. 'Coordination of Rho GTPase activities during cell protrusion'. In: *Nature* 461.7260 (Sept. 2009). Number: 7260 Publisher: Nature Publishing Group, pp. 99–103. DOI: 10.1038/nature08242.

[102] Eugene Tkachenko et al. 'Protein kinase A governs a RhoA–RhoGDI protrusion–retraction pacemaker in migrating cells'. In: *Nature Cell Biology* 13.6 (June 2011). Number: 6 Publisher: Nature Publishing Group, pp. 660–667. DOI: 10.1038/ncb2231.

[103] Chiara Malinverno et al. 'Endocytic reawakening of motility in jammed epithelia'. In: *Nature Materials* 16.5 (May 2017). Number: 5 Publisher: Nature Publishing Group, pp. 587–596. DOI: 10.1038/nmat4848.

[104] Abhijeet Joshi et al. 'The interplay between activity and filament flexibility determines the emergent properties of active nematics'. In: *Soft Matter* 15.1 (2019). Publisher: Royal Society of Chemistry, pp. 94–101. DOI: 10.1039/C8SM02202J.

[105] R. Kemkemer et al. 'Elastic properties of nematoid arrangements formed by amoeboid cells'. In: *The European Physical Journal E* 1.2 (2000), p. 215. DOI: 10.1007/s101890050024.

[106] He Li et al. 'Data-driven quantitative modeling of bacterial active nematics'. In: *Proceedings of the National Academy of Sciences* 116.3 (15th Jan. 2019). Publisher: Proceedings of the National Academy of Sciences, pp. 777–785. DOI: 10.1073/pnas.1812570116.

[107] Anupam Sengupta. 'Microbial Active Matter: A Topological Framework'. In: *Frontiers in Physics* 8 (23rd June 2020), p. 184. DOI: 10.3389/fphy.2020.00184.

[108] Carles Blanch-Mercader et al. 'Integer topological defects of cell monolayers: Mechanics and flows'. In: *Physical Review E* 103.1 (12th Jan. 2021), p. 012405. DOI: 10.1103/PhysRevE.103.012405.